



**A NEW APPROACH ON THE TECTONOMETAMORPHIC  
MECHANISMS ASSOCIATED WITH P-T PATHS OF THE  
BARROVIAN-TYPE SILGARÁ FORMATION AT THE  
CENTRAL SANTANDER MASSIF, COLOMBIAN ANDES**

*Castellanos A. Óscar M.<sup>1</sup>, Ríos R. Carlos A.<sup>2</sup> and Takasu Akira<sup>3</sup>*

<sup>1</sup> Programa de Geología, Universidad de Pamplona, Colombia. [ocastellanos@unipamplona.edu.co](mailto:ocastellanos@unipamplona.edu.co)

<sup>2</sup> Escuela de Geología, Universidad Industrial de Santander, Colombia.

<sup>3</sup> Geosciences Department, Shimane University, Matsue, Japan.

---

**ABSTRACT**

Metamorphic pressure and temperature trajectories are generally used as tools to interpret the tectonic history of deformed belts of rocks that record past activity along active plate margins. The pre-Devonian metamorphic sequence of the Silgará Formation forms part of the ancient basement of the central Santander Massif, including pelitic schists, siliceous schists and intercalation of amphibolites accompanied by marble. This metasedimentary unit has been affected by Barrovian type metamorphism under middle-pressure/high-temperature conditions. This paper presents on the relationship of tectonic processes to pressure-temperature paths development. Detailed petrologic analysis of pelites and related rocks has been used to constrain the P-T history of this region in the eastern colombian cordillera. Mineral assemblages and Geothermobarometric calculations indicate metamorphic temperatures and pressures of 400-600 °C and 4.0-6.5 kbar, respectively.

**Key words:** central Santander Massif, Silgará Formation, Barrovian type metamorphism, pelitic rocks, petrologic analysis, geothermobarometry.

---

**RESUMEN**

Las trayectorias de presión y temperatura de metamorfismo generalmente son usadas como herramientas para interpretar la historia tectónica de cinturones de rocas deformadas que registran antigua actividad a lo largo de bordes de placa activos. La secuencia pre-Devónica de la Formación Silgará forma parte del antiguo basamento que aflora en la región central del Macizo de Santander, incluyendo esquistos pelíticos, esquistos silíceos con intercalación de anfibolitas acompañadas por mármol. Esta secuencia metasedimentaria ha sido afectada por un

---

Manuscript receiver: May 30th, 2008.

Accepted for publication: August 24<sup>th</sup>, 2008

metamorfismo tipo Barroviense en condiciones de presión intermedia / temperatura alta. Este artículo especula sobre la relación entre los procesos tectónicos y el desarrollo de trayectorias de P-T. Un análisis petrológico detallado de las pelitas y rocas relacionadas ha sido usado para deducir la historia de P-T de esta región. Las paragénesis minerales y los cálculos geotermobarométricos indican temperaturas y presiones metamórficas de 400-600 °C y 4.0-6.5 kbar, respectivamente.

**Palabras clave:** región central del Macizo de Santander, Formación Silgará, Metamorfismo tipo Barroviense, rocas pelíticas, Análisis petrológico, geotermobarometría.

## Introduction

The geological evolution of the Colombian Andes (Figure 1) has been interpreted as a composite margin made up of successively accreted terranes and oceanic island arc sequences from Paleozoic to Miocene ages (Weber *et al.*, 2002), and the most important events took place during Devonian-Carboniferous and Cretaceous times (Restrepo and Toussaint, 1988). The Colombian Andes are divided into three mountain ranges, which from east to west comprise the Eastern, Central and Western Cordilleras, showing different tectonic histories and configurations. According to Cooper *et al.* (1995), the first two correspond to modern and ancient fold-thrust belts, respectively, and the last one represents an accreted arc. The Eastern Cordillera splits by the southern termination of the left-lateral strike-slip Santa Marta - Bucaramanga fault and the NW-SE trending Santander Massif into two branches that form the Perijá Range in the west and the Mérida Andes in the east.

Ward *et al.* (1973) did a detailed study on the regional geology of the Santander Massif. The Santander Massif exposes its metamorphic basement, which is composed by deformed and metamorphosed rocks that have been tectono-stratigraphically divided into three metamorphic units (Bucaramanga Gneiss Complex, Silgará Formation and Orthogneiss) and cut by intrusive bodies the emplacements of which record Caledonian to Jurassic magmatic events (Goldsmith *et al.*, 1971; Banks *et al.*, 1985; Boinet *et al.*, 1985; Dörr *et al.*, 1995; Restrepo-Pace, 1995; Ordoñez, 2003; Ordoñez and Mantilla, 2005). The Bucaramanga Gneiss Complex

is a sequence of high-grade metamorphic rocks (up to the upper amphibolite facies), which is mainly composed of pelitic gneisses with minor amounts of amphibolites and orthogneisses, and in part migmatitic. The Silgará Formation is a metamorphic sequence of low- and middle-grade (greenschist and lower amphibolite facies), which consists of meta-siliceous rocks with intercalations of orthoamphibolites intruded by granitoids and gabbros. A Gneissose granite (Orthogneiss unit) intrudes into the Bucaramanga Gneiss Complex and a wide zone of migmatite is developed around it. The Orthogneiss unit generally shows concordant foliation and lineation with those of neighboring metamorphic rocks of the Bucaramanga Gneiss Complex the Silgará Formation. According to Restrepo-Pace *et al.* (1997), the K-Ar hornblende ages of  $945 \pm 140$  Ma from hornblende gneiss (Goldsmith *et al.*, 1971) and Rb-Sr whole-rock of  $680 \pm 140$  Ma from biotite gneiss (Goldsmith *et al.*, 1971)  $^{40}\text{Ar}/^{39}\text{Ar}$  hornblende of  $668 \pm 9$  Ma and  $574 \pm 8$  Ma from hornblende gneisses (Restrepo-Pace, 1995; Restrepo-Pace *et al.*, 1997), suggests a Nickeriense tectono-metamorphic event. A tectono-metamorphic event during the Early to Middle Ordovician affected the pelitic protolith of the Silgará Formation and a series of syn-tectonic granites, according to ages Rb-Sr whole-rock of  $450 \pm 80$  Ma from gneiss and K-Ar hornblende of  $413 \pm 30$  Ma from metadiorite (Goldsmith *et al.*, 1971), U-Pb zircon of 417 Ma and 392 Ma (Banks *et al.*, 1985) and U-Pb zircon of  $477 \pm 16$  Ma (Restrepo-Pace, 1995). This event has been associated with the Caparonensis orogenic cycle in the Mérida Andes (González de Juana *et al.*, 1950), which was accompanied by several syn-tectonic in-



**Figure 1.** Map of northern South America showing major structural features. 1: Oca - El Pilar Fault System; 2: Sierra Nevada de Santa Marta; 3: Santa Marta - Bucaramanga Fault System; 4: Perijá Range; 5: Mérida Andes; 6: Eastern Cordillera; 7: Central Cordillera; 8: Western Cordillera; 9: Baudo Range; 10: Macarena Range; 11: Guaycaramo Fault System. The Santander Massif and the study area are indicated by a shadow area and by a white rectangle, respectively.

trusions with ages between 460 and 480 Ma (Restrepo-Pace, 1995), and may be correlated with the Caledonian orogeny, which was characterized by folding, metamorphism and uplift. The basement of the Santander Massif is unconformably overlain by unmetamorphosed rocks of the Middle Devonian

Floresta Formation. The lack of regional metamorphism in the Devonian sedimentary units suggests that the last metamorphic event in the eastern Colombian Andes occurred before the beginning of deposition of the Upper Emsian beds (Forero, 1990). Silurian fossils [brachiopod *Aenigmastrophia* sp.

(Ludlowian)] are present in low-grade metamorphic rocks of the Santander Massif near Guaca (Forero, 1990). The basement of the Santander Massif is unconformably overlaid by unmetamorphosed rocks of the Middle Devonian Floresta Formation. Carboniferous and Permian clastic to calcareous sediments unconformably overlay this unit. Due to pre-Cretaceous erosional events, these Paleozoic sequences are restricted in their occurrence (Kammer, 1993). At the end of the Late Paleozoic orogenic event, calc-alkaline batholiths (Santander Plutonic Complex) were intruded during the Triassic-Jurassic time. Several K-Ar ages on biotite from plutons and batholiths that crop out in the Santander Massif reflect a magmatic event during the Late Triassic - Early Jurassic. The regional isograds are not parallel to the outline of the intrusive rocks. The orthogneisses exhibit concordant relationships with the high-grade metamorphic rocks, and may be interpreted as syn-tectonic intrusives emplaced at close to the peak metamorphism. Post-Paleozoic sediments, which overlay the Upper Paleozoic marine sediments, include the Bocas and Jordán formations. The latter consists of fine-grained red beds with interlayered volcanic rocks and intrusive clasts, a is discordantly overlaid by the red bed sequence of the Girón Formation of Jurassic age. Cretaceous sedimentary rocks occur around the Santander Massif and are preserved as erosional relicts. The structural setting of the Santander Massif is dominated by complex faulting, and the most conspicuous fault is the active north-west-trending linear left-lateral strike-slip Bucaramanga - Santa Marta Fault, which appears to have had a long history (Goldsmith *et al.*, 1971). In the last 20 years, the metamorphic rocks of the Santander Massif have been the focus of attention of an increasing number of studies (e.g., Restrepo-Pace, 1995; Restrepo-Pace *et al.*, 1997; Schäfer *et al.*, 1998; García y Ríos, 1997, 1998; García y Castellanos, 1998; Campos, 1999; García y Ríos, 1999; Montenegro y Barragán, 1999; Ríos, 1999, 2001; Ríos and Takasu, 1999, 2000; Ríos and García, 2001a, 2001b; García y Campos, 2000; Castellanos, 2001; Mantilla *et al.*, 2001; 2002; 2003; Gélvez and Márquez, 2002; Ríos *et al.*, 2003a, 2003b; Cardona,

2003; Castellanos *et al.*, 2004; García *et al.*, 2005; Ríos, 2005; Gómez y Ávila, 2006), which have contributed to its geological knowledge and pointed out the importance of this ancient massif as a key for understanding the complex geotectonic evolution of the northwestern continental margin of South America. These studies define a regional metamorphism of middle to high grade that reaches the upper amphibolite facies and varies according to the region in the massif. In this paper, we present petrological data for the Silgará Formation metapelitic rocks that crop out at the Central Santander Massif (CSM). We examine metamorphic textures and mineral assemblages to establish the stages of evolution of the metamorphism, use phase diagram analysis and P-T grid to study the sequence of mineral assemblages and reaction history, and apply the GTB program of Spear and Kohn (2001) to estimate metamorphic P-T conditions and define the P-T paths experienced by the Silgará Formation pelitic rocks. However, further studies should integrate this information with both previously published data and structural and geochronological data in order to improve our knowledge of this metamorphic unit and constraint on its tectono-metamorphic evolution in the geological context of the Colombian Andes.

## Geological setting

In the CSM, two distinct geological domains constitute the crystalline basement (Figure 2): the deformed and metamorphosed rocks of the Bucaramanga Gneiss Complex, Silgará Formation and Orthogneiss and the igneous succession developed after (1) syn-orogenic magmatism with alkaline affinity during the Paleozoic and (2) post-orogenic magmatism with calc-alkaline affinity during Triassic-Jurassic (Goldsmith *et al.*, 1971; Banks *et al.*, 1985; Boinet *et al.*, 1985; Dörr *et al.*, 1995; Restrepo-Pace, 1995; Ordoñez, 2003; Ordoñez and Mantilla, 2005). The rocks of interest in this study are referred to as the Lower Paleozoic metamorphic sequence of the Silgará Formation that crops out in two N-S trending strips and is interrupted by the presence of dykes and sills of orthoamphibolites with banded

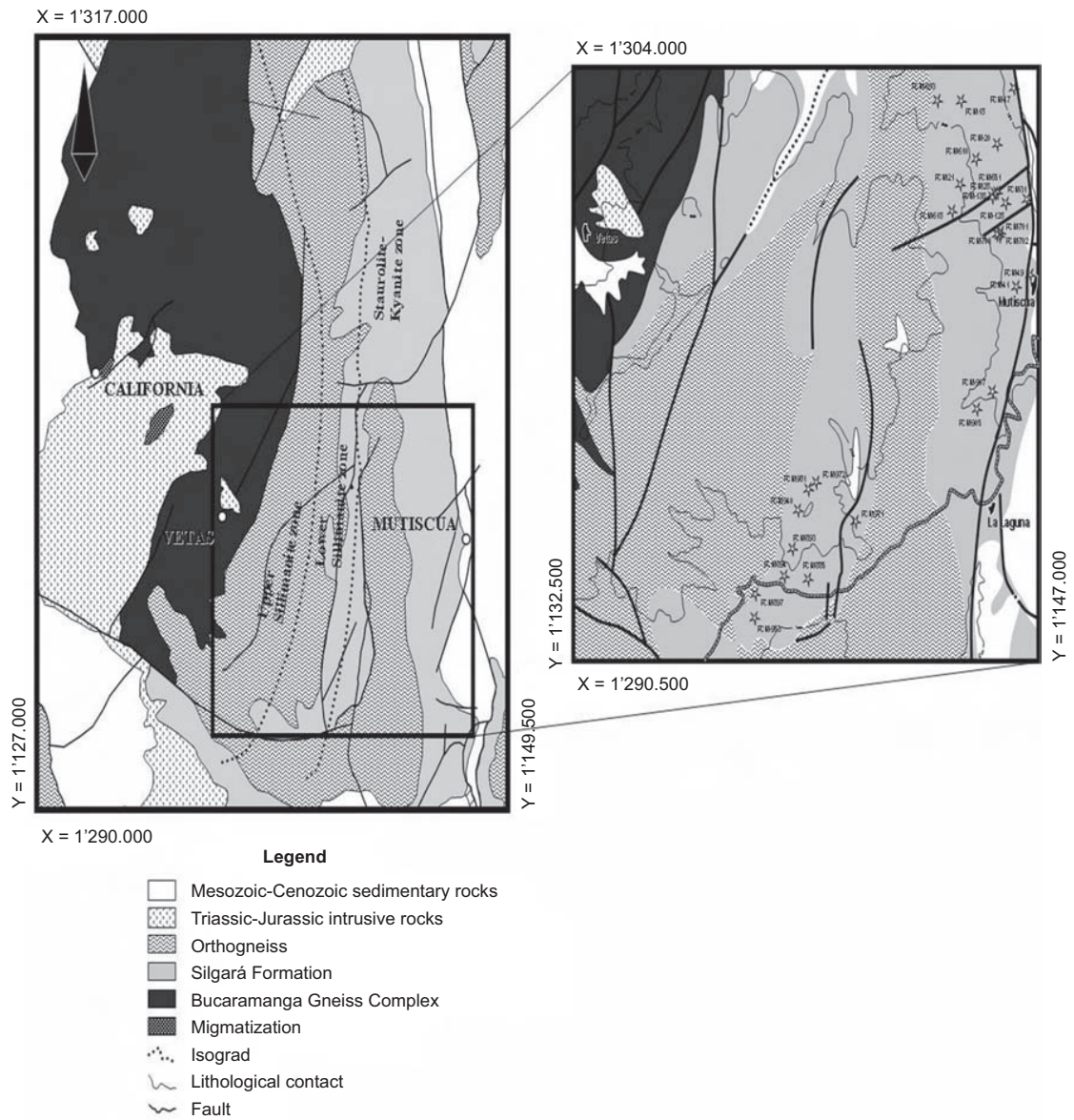


**Figure 2.** Generalized geological map of the CSM modified after Ward *et al.*, (1970) and García *et al.*, (2005), showing the study area as well as the sampling localities of metapelitic rocks of the Silgará Formation.

to gabbroic structures. The Silgará Formation is mainly composed of metapelitic rocks with minor intercalated psammitic, semipelitic, metabasic and metacarbonate rocks (Figure 3), which were affected by a Caledonian regional metamorphism that produced metamorphic zonation ranging from the biotite zone through the garnet and staurolite-kyanite zones up to the sillimanite zone of the typical Barrovian

zonal scheme under low- to high-temperature and medium-pressure conditions. Gómez y Avila (2006) carried out a study of the metamorphic sequence cropping out along the Valegra stream, making emphasis on the metacarbonate and associated rocks that occur in the contact between marble and polite layers. A broad spectrum of physical conditions, varying from greenschist facies to amphibolite fa-

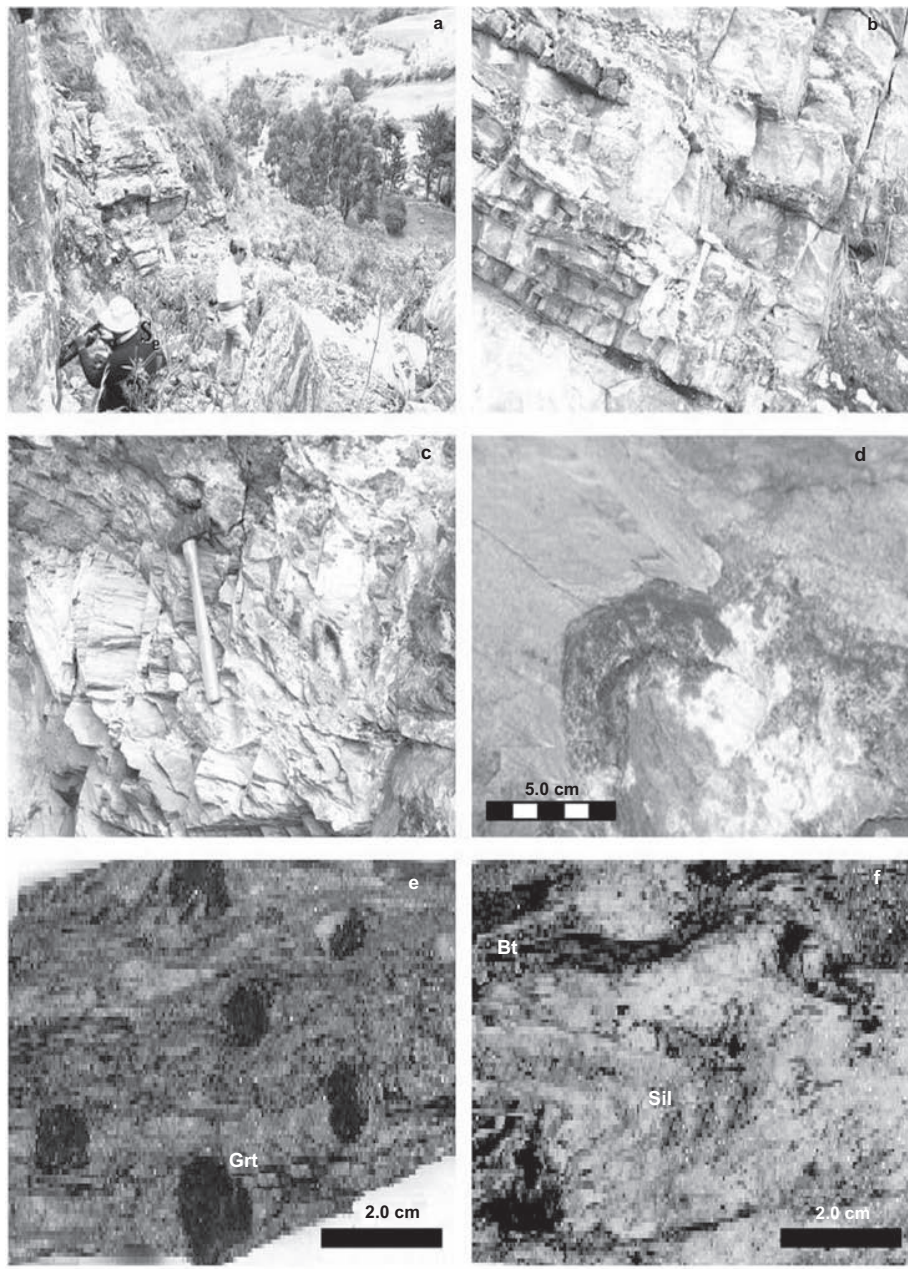


**Figure 3.** Field and hand-specimen photographs from the Silgará Formation metamorphic rocks at the CSM. (a) Outcrop of marble quarry in which marble and amphibolite are interlayered with pelitic rocks. (b) Metacarbonate rocks (pure and impure marbles, carbonate-silicate rocks, calc-silicate rocks and carbonate-bearing silicate rocks), which form a very complex group within the metamorphic sequence. (c) Garnet-bearing pelitic schists displaying a pervasively schistosity, which represent the most common type of metamorphic rock. (d) Recumbent fold (with a subhorizontal axial plane strikes N40°W and dipping 25°NE) in marble interlayered with pelitic schists. (e) Polished hand specimen of a pelitic schist (sample PCM-971), showing schistose structure and the largest garnet porphyroblasts in the study area, alternating with non-continuous quartz-rich bands. (f) Polished hand specimen of a pelite (PCM-940), showing a schistose and microfolding (tight structure) with a millimeter-scale compositional banding of alternating and non-continuous biotite and sillimanite bands.

cies, have been attributed to the investigated metamorphic sequence. Recent studies (Campos, 1999; García y Ríos, 1999; Montenegro y Barragán, 1999; García y Campos, 2000; Castellanos, 2001; Castellanos *et al.*, 2004; García *et al.*, 2005) reveal a complex metamorphic and deformational history for this geological unit. Castellanos (2001) determined the P-T conditions for the high-T and medium-P facies series terrane at the CSM. Recently, García *et al.* (2005) defined a clockwise P-T path followed by the metamorphic basement in this region. However, regarding to the tectono-metamorphic evolution of the Silgará Formation, few studies have been done so far. Here, we re-examine the metapelitic rocks of this metamorphic unit because they are highly sensitive to changes in pressure and temperature conditions and preserve textural, structural and mineralogical evidence that provide important clues to constrain the tectono-metamorphic evolution of the Silgará Formation at the CSM, because they preserve mineral assemblages from different tectonic events that are appropriate for determining the metamorphic P-T conditions. These rocks show overprinting relationships allowing the recognition of three main deformation events ( $D_1$ ,  $D_2$ , and  $D_3$ ) at the CSM, and during the last stage they were affected by an extensive retrograde metamorphism. The first deformation phase  $D_1$  may be associated to crustal shortening and thickening, developing  $S_1$ . The  $D_1$  deformational fabrics sometimes are poorly preserved due to overprinting and transposition by subsequent deformational events. However, evidence for this event, which is characterized by the mineral assemblage quartz + ilmenite + graphite  $\pm$  muscovite, includes both inclusion trails in garnet or staurolite porphyroblasts and differentiated layering in hinge zones, defined by alternating phyllosilicate- and quartz-feldspathic-rich layers. Deformation  $D_2$  as a result of heating and thrusting developed a dominant schistosity ( $S_2$ ), which is the regional foliation formed at the same time with the first-generation of folds and thrusts, and represented by the mineral assemblage quartz + muscovite + biotite + ilmenite + garnet + staurolite + kyanite  $\pm$  andalusite  $\pm$  plagioclase. Regional-scale ductile shear zones with

a mylonitic foliation parallel to the regional foliation ( $S_2$ ) are associated with  $D_2$ .  $D_3$  has also resulted in the folding or crenulation of  $S_2$  and the development of a weak spaced cleavage ( $S_3$ ), which is represented by the mineral assemblage quartz + sillimanite + biotite + garnet. In general, later structures such as flat-lying crenulations, small chevron folds and kink bands overprint the main foliation =  $D_3$ ?. The most recent deformation is observed in all lithologies and has produced the development of tectonites, which could be associated to younger structures such as faulting. A final movement along this tectonic discontinuity is post- $D_3$ . This phase of deformation may be corresponding to the last uplift of the Eastern Cordillera the Middle Miocene.

### Petrography and mineral chemistry

To constrain the P-T conditions of metamorphism of the Silgará Formation at the CSM, 60 samples of metapelitic rocks were petrographically studied. Metapelites display a well-developed schistosity defined by the preferred orientation of muscovite and biotite flakes. The schistosity is also due to the alignment of phyllosilicate flakes and crystals of opaque minerals or graphite, sometimes along with aggregates of aluminosilicates, mainly kyanite and sillimanite (fibrolite). Biotite is not only present as small flakes underlying the planar structure but also as lozenge-shaped crystals which represent early porphyroblasts and their asymmetry is sometimes different to useful to determine sense of shear. A last generation of biotite appears as undeformed crystals with their cleavage perpendicular or randomly oriented to the schistosity and can be interpreted as postkinematic. Quartz and plagioclase form granoblastic-rich fabrics between the mica-rich fabrics. Garnets commonly occur as euhedral to subhedral porphyroblasts; their cores are frequently rich in small inclusions of quartz, plagioclase, opaque minerals and graphite, and their rims are poorer in inclusions. In some cases, inclusion patterns define an internal foliation ( $S_i$ ) an external foliation ( $S_e$ ) = ( $S_2$ )?, producing sigmoidal inclusions. Staurolite occurs as porphyroblasts elongated in the

foliation, usually showing sigmoidal patterns of inclusions that indicate a synkinematic crystallization, and as porphyroblasts oriented across the foliation that indicate post-kinematic crystallization. Both generations of staurolite are rich in quartz and opaque mineral inclusions, although graphite also occurs. Accessory mineral phases include opaque minerals, graphite, epidote, apatite and zircon. Small scale folding of the schistosity planes has produced a crenulation cleavage, accompanied by segregation of quartz into horizontal layers. These rocks frequently contain evidence of retrograde metamorphism, involving hydration processes, including partial replacement of garnet, biotite and staurolite by chlorite, staurolite by white mica and plagioclase and staurolite by sericite. Figures 4 and 5 illustrate the main petrographical aspects of the investigated Silgará Formation pelites. Mineral abbreviations are after Kretz (1983). Mineral compositions were analyzed using a JEOL JXA 8800M electron microprobe analyzer at the Geosciences Department of Shimane University (Japan), under the following analytical conditions: accelerating voltage 15 kV, specimen current  $2.5 \times 10^{-8}$  A, correction method after Bence and Albee (1968). Representative analyses of mineral phases are given in Tables 1 to 6.

Muscovite shows a subidioblastic character, and is usually colorless. In general, it shows straight and serrated boundaries and develops a directional lepidoblastic fabric. It is associated with biotite and chlorite. The first type of muscovite occurs as aggregates in the lepidoblastic bands defining the main schistosity of the rock. In some cases bands are deformed following the shape of porphyroblasts of garnet, plagioclase, staurolite or aluminosilicates. It is sometimes replaced by fibrolite. The second type of muscovite occurs as porphyroblasts or within the lepidoblastic bands, and contains inclusions of opaque minerals, quartz and enclosed relicts of staurolite suggesting retrograde metamorphism. The third type of muscovite, occurs as random distributed and oriented inclusions in plagioclase, staurolite, quartz and garnet. The mineral chemistry of muscovite is depicted in Table 1 and illustrated in Figure 6. The Si content is 5.94-6.39 p.f.u. based on 22 anhy-

drous oxygens (Deer et al., 1982). The compositions of muscovite,  $X_{Na}=Na/(Na+K)$  varies from 0.02 to 0.36. Muscovites from the mineral assemblages St+Grt and Ky+And+Sil shown two groups, one with higher  $X_{Na}$  than the average from the other samples.

Biotite shows a subidioblastic character, occurs as aggregates in thin and thick bands, and also as individual grains of different sizes, and as small inclusions in garnet, staurolite and plagioclase. In some cases porphyroblasts are parallel or completely perpendicular to  $S_e$ , suggesting post-tectonic growth for the second case. It shows invariably brown in color, a mottled appearance, straight and serrated boundaries and pleochroism x: dark brown, y: pale brown, z: brown. Sometimes biotite is partial to totally replaced by chlorite. The mineral chemistry of biotite is depicted in Table 2. The Fe/(Fe+Mg) ratio of biotite ranges from 0.37 to 0.79 and  $Al^{IV}$  varies from 2.50 to 2.83. Biotite from samples PCM-18, PCM-49 and PCM-610 shown Fe/(Fe+Mg) ratios ranging from 0.24 to 0.30 and  $Al^{IV}$  varies from 2.27 to 2.58, corresponding to phlogopite component. Ti content varies from 0.93-3.31. However, no relation was found between content of Ti in biotite and grade of metamorphism.

Chlorite is considered to be a retrograde phase after biotite, garnet and amphibole. Si content is 5.05-5.95 p.f.u. based on 28 anhydrous oxygens, and  $X_{Mg}$  varies between 0.30 and 0.74.

Garnet occurs as porphyroblasts with idioblastic to xenoblastic character. It is also possible to distinguish two types of garnets according to their texture: poikiloblastic and sector zoned garnets. They sometimes show a trail of inclusions of quartz, graphite and opaque minerals almost perpendicular to the  $S_e$  of the rock, and most are partially included in staurolite porphyroblasts. Some garnets are sub-rounded to rounded and show a rotational trail of inclusions of quartz or S-shaped spiral structure. Garnets rarely show concordant internal schistosity trails of inclusions of quartz and opaque minerals. In addition, poikiloblastic garnets in some samples show elongated shape suggesting dendritic character possibly due to high rate of growth. The mineral chemistry



**Table 2.** Representative Chemicals compositions of biotite from pelitic Rocks of the Silgará Fomation at the CSM.

Lithology	PS	PS	PS	PS	PS	PS	PS	PS	PS	PS	PS	PS	PS	PS	PS	PS	PS	PS
Sample No.	PCM-18	PCM-20	PCM-21	PCM-28	PCM-49	PCM-610	PCM-618	PCM-651	PCM-885	PCM-893	PCM-894	PCM-897	PCM-940	PCM-953	PCM-971	PCM-972		
Analysis No.	1	1	1	1	1	2	10	1	1	1	1	1	1	1	4	1		
Weight %	Inc. Bt	matrix	matrix	matrix	matrix	matrix	matrix	matrix	matrix	matrix	matrix	matrix	matrix	matrix	matrix	matrix		
SiO <sub>2</sub>	36.95	36.98	36.57	35.70	39.67	38.20	35.00	34.92	33.10	33.85	34.77	34.19	34.84	34.74	34.29	33.61		
TiO <sub>3</sub>	1.08	1.37	1.24	1.41	0.93	0.96	2.51	2.08	1.95	2.91	2.88	3.08	3.01	3.07	2.71	2.98		
Al <sub>2</sub> O <sub>3</sub>	18.92	18.19	19.48	18.56	18.73	20.49	18.63	19.35	17.81	19.61	18.94	18.05	19.75	19.40	19.25	19.62		
FeO*	10.78	14.75	15.16	18.35	11.84	10.52	20.73	20.19	27.57	21.05	18.65	22.45	20.01	19.57	21.17	21.30		
MnO	0.40	0.02	0.18	0.00	0.27	0.16	0.01	0.03	0.23	0.19	0.31	0.31	0.22	0.30	0.11	0.31		
MgO	16.79	14.04	13.21	11.91	15.26	18.55	8.09	9.33	4.21	7.87	9.20	7.93	8.62	8.16	7.22	7.98		
Na <sub>2</sub> O	0.47	0.57	0.41	0.47	0.37	0.13	0.46	0.38	0.17	0.40	0.36	0.49	0.39	0.34	0.35	0.42		
K <sub>2</sub> O	8.75	9.15	8.36	8.86	8.18	6.67	8.95	9.39	9.75	9.53	10.25	10.08	9.67	9.61	9.19	9.71		
Total	94.20	95.07	94.61	95.30	95.33	95.74	94.38	95.71	94.79	95.48	95.36	96.57	96.52	95.23	94.29	96.04		
<b>Cations per 22 Oxygens</b>																		
Si	5.438	5.502	5.447	5.395	5.727	5.418	5.412	5.321	5.334	5.215	5.319	5.271	5.270	5.319	5.334	5.167		
Ti	0.119	0.153	0.138	0.160	0.101	0.102	0.292	0.238	0.236	0.337	0.332	0.357	0.342	0.354	0.317	0.345		
Al	3.282	3.190	3.420	3.306	3.187	3.425	3.396	3.474	3.383	3.562	3.414	3.280	3.520	3.501	3.528	3.556		
Fe <sup>2+</sup>	1.327	1.835	1.888	2.319	1.429	1.248	2.680	2.572	3.715	2.712	2.385	2.895	2.531	2.505	2.753	2.739		
Mn	0.049	0.003	0.023	0.000	0.033	0.019	0.001	0.004	0.031	0.024	0.040	0.040	0.028	0.039	0.014	0.040		
Mg	3.684	3.115	2.933	2.683	3.284	3.922	1.866	2.119	1.010	1.807	2.097	1.823	1.943	1.862	1.674	1.830		
Na	0.134	0.164	0.119	0.138	0.104	0.037	0.139	0.112	0.053	0.120	0.107	0.147	0.113	0.101	0.106	1.124		
K	1.642	1.736	1.588	1.708	1.506	1.206	1.765	1.825	2.003	1.873	1.999	1.982	1.866	1.877	1.822	1.905		
Total	15.687	15.699	15.558	15.714	15.382	15.389	15.550	15.671	15.766	15.660	15.695	15.795	15.616	15.563	15.549	15.721		

\* Total Fe as FeO.

**Table 3.** Representative Chemicals compositions of biotite from pelitic Rocks of the Silgará Fomation at the CSM.

Lithology Sample No.	PS PCM-47			PS PCM-618				PS PCM-651		PS PCM-700		PS PCM-701		PS PCM-702		PS PCM-953	
	3	12	rim	1P	2P	5SZ	6SZ	14	13	1	7	9	16	1	7	1	18
Analysis No.	mantle	rim	core	rim	rim	core	core	core	rim	core	rim	core	rim	core	rim	core	mantle
Weight %	36.44	37.10	37.06	37.31	36.84	36.58	36.58	37.74	37.51	36.07	36.10	36.68	36.52	36.70	37.06	37.31	37.28
SiO <sub>2</sub>	0.14	0.02	0.01	0.00	0.00	0.01	0.01	0.04	0.02	0.02	0.04	0.03	0.04	0.00	0.00	0.00	0.02
TiO <sub>2</sub>	20.23	20.57	21.02	21.22	20.68	20.62	21.01	21.11	21.11	19.95	20.16	20.36	20.45	20.46	20.73	21.03	21.08
Al <sub>2</sub> O <sub>3</sub>	33.69	35.66	36.28	36.28	34.75	35.23	34.29	34.72	41.06	41.55	41.55	38.08	38.83	37.09	39.13	31.24	34.67
FeO*	4.04	1.49	0.79	0.33	0.10	0.99	1.07	0.16	0.03	0.03	0.02	0.88	0.31	1.62	0.19	6.07	2.46
MnO	1.88	3.06	2.53	2.89	2.69	1.76	2.69	3.01	1.37	1.39	1.39	1.57	1.82	1.72	2.49	1.96	3.05
MgO	3.46	2.66	2.92	2.81	3.31	3.59	4.09	3.35	0.37	0.31	0.31	1.58	1.09	1.62	0.77	2.97	1.99
CaO	0.01	0.01	0.00	0.05	0.04	0.00	0.00	0.02	0.07	0.01	0.01	0.01	0.09	0.00	0.05	0.11	0.00
Na <sub>2</sub> O	0.01	0.05	0.05	0.01	0.01	0.03	0.03	0.05	0.01	0.05	0.05	0.05	0.04	0.04	0.05	0.04	0.02
K <sub>2</sub> O	0.00	0.00	0.00	0.01	0.01	0.02	0.03	0.01	0.01	0.01	0.00	0.00	0.00	0.00	0.02	0.01	0.00
Cr <sub>2</sub> O <sub>3</sub>	99.90	100.60	100.76	100.91	98.44	98.82	100.99	99.95	98.96	99.63	99.24	99.15	99.25	100.48	100.74	100.58	100.58
Total	2.975	2.987	2.979	2.983	3.009	2.998	3.006	3.008	3.000	2.987	3.015	3.004	3.011	3.001	3.002	2.990	2.990
Si	0.009	0.001	0.001	0.000	0.000	0.001	0.003	0.001	0.001	0.002	0.002	0.002	0.000	0.000	0.000	0.001	0.001
Ti	1.947	1.51	1.992	2.000	1.990	1.992	1.971	1.995	1.956	1.965	1.972	1.983	1.979	1.979	1.993	1.992	1.992
Al	0.085	0.074	0.049	0.034	0.000	0.011	0.012	0.000	0.041	0.057	0.000	0.004	0.000	0.000	0.003	0.025	0.025
Fe <sup>3+</sup>	2.216	2.326	2.396	2.392	2.373	2.403	2.272	2.329	2.815	2.818	2.617	2.668	2.545	2.629	2.098	2.300	2.300
Fe <sup>2+</sup>	0.279	0.102	0.054	0.022	0.007	0.069	0.072	0.011	0.002	0.001	0.061	0.022	0.112	0.013	0.414	0.167	0.167
Mn	0.229	0.367	0.303	0.345	0.327	0.215	0.319	0.360	0.170	0.171	0.192	0.223	0.210	0.301	0.235	0.365	0.365
Mg	0.303	0.229	0.251	0.241	0.290	0.315	0.349	0.287	0.033	0.027	0.139	0.096	0.142	0.066	0.256	0.171	0.171
Ca	0.004	0.003	0.000	0.016	0.014	0.000	0.000	0.005	0.023	0.004	0.002	0.029	0.001	0.015	0.036	0.000	0.000
Na	0.003	0.010	0.011	0.002	0.003	0.006	0.007	0.010	0.003	0.011	0.010	0.009	0.009	0.011	0.009	0.004	0.004
K	0.000	0.000	0.000	0.001	0.001	0.001	0.002	0.001	0.001	0.000	0.000	0.000	0.000	0.001	0.000	0.000	0.000
Cr	8.049	8.050	8.036	8.035	8.013	8.011	8.012	8.007	8.046	8.044	8.010	8.039	8.009	8.036	8.046	8.017	8.017
Total	8.049	8.050	8.036	8.035	8.013	8.011	8.012	8.007	8.046	8.044	8.010	8.039	8.009	8.036	8.046	8.017	8.017

Cations per 12 O

\* Total Fe as FeO<sub>2</sub>

**Table 4.** Representative Chemicals compositions of Staurolite from pelitic Rocks of the Silgará Fomation at the CSM.

Lithology	PS	PS	PS	PS	PS	PS	PS	PS	PS	PS	PS	PS	PS	PS	PS	PS	PS
Sample No.	PCM-20	PCM-21	PCM-47	PCM-49	PCM-618	PCM-651	PCM-700	PCM-701	PCM-702	PCM-905	PCM-907	PCM-940	PCM-971				
Analysis No.	8	1	7	3	4	8	2	18	8	7	4	5	4				
Weight %																	
SiO <sub>2</sub>	26.95	27.94	27.86	27.74	26.55	27.56	26.44	26.97	28.62	27.31	27.11	26.54	26.68				
TiO <sub>2</sub>	0.46	0.46	0.52	0.40	0.52	0.63	0.64	0.70	0.55	0.58	0.52	0.81	0.60				
Al <sub>2</sub> O <sub>3</sub>	54.44	52.81	53.17	52.77	54.48	52.68	53.64	53.78	51.85	52.97	53.33	53.76	53.17				
FeO*	13.43	12.79	13.80	9.22	13.19	14.50	13.94	14.76	14.97	13.79	13.84	13.16	14.05				
MnO	0.02	0.50	0.05	1.24	0.01	0.05	0.01	0.03	0.03	0.29	0.41	0.64	0.15				
MgO	2.42	2.27	1.81	2.39	1.21	1.55	0.92	1.52	1.45	1.94	1.89	1.54	1.28				
CaO	0.03	0.00	0.00	0.02	0.00	0.00	0.00	0.00	0.02	0.02	0.00	0.01	0.00				
Na <sub>2</sub> O	0.02	0.00	0.02	0.14	0.08	0.01	0.01	0.00	0.00	0.03	0.00	0.07	0.07				
K <sub>2</sub> O	0.01	0.03	0.03	0.03	0.04	0.02	0.01	0.06	0.03	0.03	0.03	0.06	0.04				
ZnO	0.08	0.61	0.15	3.70	1.34	0.50	0.62	0.05	0.12	0.05	0.30	1.16	1.36				
Cr <sub>2</sub> O <sub>3</sub>	0.01	0.04	0.04	0.03	0.04	0.08	0.04	0.05	0.05	0.06	0.04	0.05	0.00				
Total	97.87	97.44	97.44	97.67	97.47	97.58	96.27	97.92	97.67	97.07	97.47	97.81	97.39				
<b>Cations per 23 Oxygens</b>																	
Si	3.738	3.896	3.884	3.876	3.720	3.862	3.748	3.763	3.999	3.831	3.795	3.717	3.761				
Ti	0.048	0.048	0.054	0.042	0.055	0.066	0.069	0.073	0.057	0.061	0.055	0.086	0.064				
Al	8.900	8.679	8.737	8.689	8.995	8.699	8.963	8.844	8.539	8.757	8.797	8.873	8.835				
Fe <sup>3+</sup>																	
Fe <sup>2+</sup>	1.558	1.491	1.609	1.077	1.545	1.698	1.653	1.722	1.749	1.617	1.620	1.542	1.657				
Mn	0.002	0.059	0.006	0.146	0.001	0.005	0.001	0.004	0.003	0.035	0.048	0.076	0.017				
Mg	0.500	0.471	0.377	0.498	0.253	0.325	0.194	0.316	0.301	0.406	0.394	0.322	0.268				
Ca	0.004	0.000	0.000	0.003	0.001	0.000	0.000	0.000	0.003	0.003	0.000	0.001	0.000				
Na	0.005	0.000	0.005	0.039	0.021	0.002	0.003	0.000	0.000	0.008	0.001	0.019	0.019				
K	0.002	0.005	0.005	0.005	0.001	0.004	0.001	0.011	0.005	0.005	0.005	0.011	0.007				
Zn	0.008	0.062	0.015	0.382	0.139	0.051	0.065	0.005	0.012	0.005	0.031	0.120	1.141				
Cr	0.001	0.005	0.005	0.003	0.004	0.009	0.005	0.006	0.005	0.006	0.005	0.006	0.000				
Total	14.767	14.717	14.696	14.759	14.740	14.722	14.702	14.744	14.674	14.733	14.752	14.772	14.771				

\* Total Fe as FeO

**Table 5.** Representative Chemicals compositions of  $Al_2SiO_5$  polymorphs from pelitic Rocks of the Silgará Fomation at the CSM.

Lithology Sample No.	PS (And)		PS (And)		PS (And)		PS (Ky)		PS (Ky)		PS (Sil)		PS (Sil)		PS (Sil)	
	PCM-18	PCM-20	PCM-21	PCM-49	PCM-18	PCM-20	PCM-21	PCM-49	PCM-20	PCM-49	PCM-20	PCM-53	PCM-972	PCM-981	PCM-972	PCM-981
Analysis No.	13	10	1	1	8	1	6	1	17	7	8	3				
Weight %																
SiO <sub>2</sub>	36.41	36.50	36.63	36.78	36.56	36.59	36.82	36.59	36.34	35.81	35.48	36.49				
TiO <sub>2</sub>	0.00	0.04	0.00	0.00	0.00	0.00	0.00	0.03	0.00	0.00	0.03	0.06				
Al <sub>2</sub> O <sub>3</sub>	63.80	61.86	62.83	61.93	63.25	61.70	62.63	61.30	63.26	64.05	63.84	62.18				
FeO*	0.66	0.88	0.82	0.80	0.96	0.73	0.76	0.85	0.33	0.33	0.14	0.59				
MnO	0.02	0.00	0.00	0.00	0.00	0.02	0.00	0.00	0.00	0.04	0.04	0.00				
MgO	0.01	0.01	0.00	0.00	0.00	0.00	0.02	0.01	0.00	0.00	0.03	0.19				
CaO	0.00	0.01	0.00	0.04	0.02	0.01	0.02	0.02	0.00	0.00	0.01	0.05				
Na <sub>2</sub> O	0.01	0.00	0.00	0.01	0.03	0.00	0.00	0.00	0.00	0.00	0.01	0.02				
K <sub>2</sub> O	0.04	0.04	0.01	0.05	0.02	0.05	0.01	0.03	0.04	0.03	0.03	0.30				
Cr <sub>2</sub> O <sub>3</sub>	0.04	0.05	0.03	0.04	0.02	0.06	0.02	0.00	0.03	0.03	0.00	0.03				
Total	110.98	99.38	100.33	99.64	100.87	99.16	100.27	98.81	100.00	100.28	99.59	99.90				
<b>Cations per 5 O</b>																
Si	0.977	0.996	0.990	1.000	0.984	1.000	0.995	1.003	0.983	0.967	0.964	0.991				
Ti	0.000	0.001	0.000	0.000	0.000	0.000	0.000	0.001	0.000	0.000	0.000	0.001				
Al	2.018	1.989	2.001	1.985	2.006	1.987	1.994	1.980	2.017	2.038	2.044	1.991				
Fe <sup>2+</sup>	0.015	0.020	0.019	0.018	0.022	0.017	0.017	0.019	0.008	0.007	0.003	0.013				
Mn	0.000	0.000	0.000	0.000	0.000	0.001	0.000	0.000	0.000	0.001	0.001	0.000				
Mg	0.001	0.000	0.000	0.000	0.000	0.000	0.001	0.001	0.000	0.000	0.001	0.008				
Ca	0.000	0.000	0.000	0.001	0.001	0.000	0.000	0.000	0.000	0.000	0.000	0.002				
Na	0.001	0.000	0.000	0.000	0.002	0.000	0.000	0.000	0.000	0.000	0.000	0.001				
7K	0.001	0.001	0.000	0.002	0.001	0.002	0.000	0.001	0.001	0.001	0.001	0.010				
Cr	0.001	0.001	0.001	0.001	0.000	0.001	0.000	0.000	0.001	0.001	0.000	0.001				
Total	3.014	3.009	3.010	3.008	3.014	3.007	3.008	3.005	3.009	3.014	3.015	3.017				

\* Total Fe as FeO

**Table 6.** Representative Chemicals compositions of plagioclase from pelitic Rocks of the Silgará Fomation at the CSM.

Lithology	PS	PS	PS	PS	PS	PS	PS	PS	PS	PS	PS	PS
Sample No.	PCM-20	PCM-21	PCM-47	PCM-49	PCM-618	PCM-651	PCM-701	PCM-702	PCM-953			
Analysis No.	1	1	3	1	3	13	1	1	1	1	1	29
Weight %	core	rim	rim	core	Inc. Grt	mantle	rim	rim	rim	rim	rim	core
SiO <sub>2</sub>	65.65	52.60	62.04	58.33	58.31	60.08	67.23	67.68	63.58	67.68	67.68	63.58
TiO <sub>2</sub>	0.00	0.00	0.02	0.00	0.00	0.00	0.02	0.00	0.00	0.00	0.00	0.00
Al <sub>2</sub> O <sub>3</sub>	21.99	29.91	23.18	26.39	25.28	24.95	19.66	19.80	21.95	19.80	19.80	21.95
FeO*	0.00	0.06	0.05	0.00	0.28	0.04	0.00	0.03	0.05	0.03	0.03	0.05
MnO	0.01	0.02	0.00	0.00	0.00	0.00	0.01	0.00	0.00	0.00	0.00	0.00
MgO	0.00	0.00	0.01	0.00	0.01	0.00	0.01	0.00	0.00	0.00	0.00	0.00
CaO	2.01	12.22	4.79	8.53	7.03	7.08	0.55	0.74	3.14	0.55	0.74	3.14
Na <sub>2</sub> O	10.26	4.38	9.05	6.78	7.62	7.53	11.52	10.37	9.97	11.52	10.37	9.97
K <sub>2</sub> O	0.11	0.09	0.14	0.09	0.15	0.13	0.12	0.10	0.36	0.12	0.10	0.36
Total	100.02	99.28	99.27	100.12	99.28	99.81	99.12	98.71	99.06	99.12	98.71	99.06
<b>Cations per 8 O</b>												
Si	2.880	2.397	2.771	2.606	2.651	2.681	2.970	2.987	2.837	2.970	2.987	2.837
Ti	0.000	0.000	0.001	0.000	0.000	0.000	0.001	0.000	0.000	0.001	0.000	0.000
Al	1.137	1.607	1.220	1.389	1.341	1.312	1.023	1.030	1.155	1.023	1.030	1.155
Fe <sup>2+</sup>	0.000	0.002	0.002	0.000	0.011	0.001	0.000	0.001	0.002	0.000	0.001	0.002
Mn	0.000	0.001	0.000	0.000	0.000	0.000	0.000	0.000	0.000	0.000	0.000	0.000
Mg	0.000	0.000	0.000	0.000	0.000	0.000	0.001	0.000	0.000	0.001	0.000	0.000
Ca	0.094	0.597	0.229	0.408	0.339	0.339	0.026	0.035	0.150	0.026	0.035	0.150
Na	0.872	0.387	0.783	0.587	0.665	0.651	0.987	0.887	0.862	0.987	0.887	0.862
K	0.006	0.005	0.008	0.005	0.009	0.007	0.007	0.005	0.021	0.007	0.005	0.021
Total	4.990	4.995	5.014	4.996	5.016	4.992	5.015	4.945	5.02	5.015	4.945	5.02

\* Total Fe as FeO

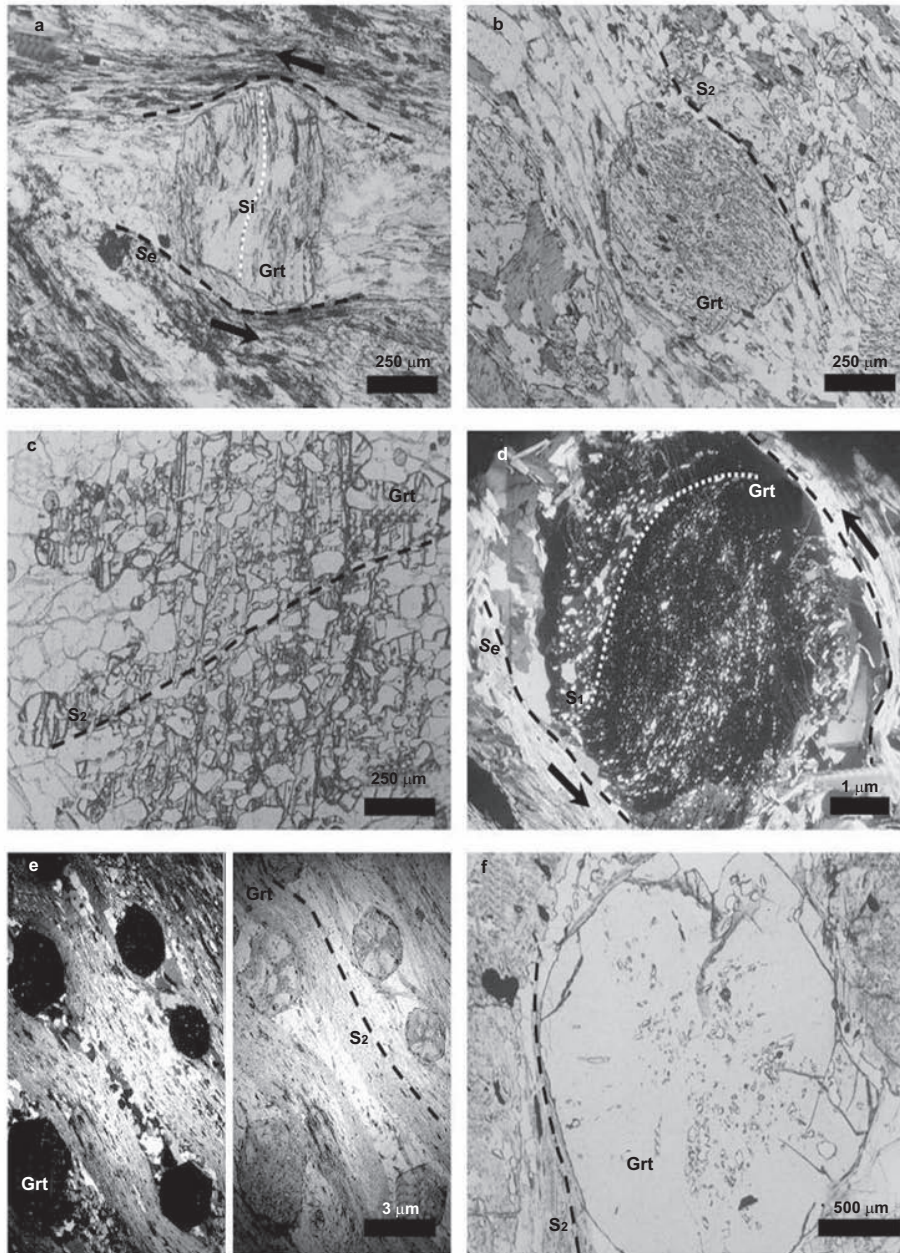


**Figure 4.** Petrographic features of the garnet-bearing pelitic rocks of the Silgará Formation at the CSM. (a) Garnet showing a pattern of inclusions of quartz, graphite and opaque minerals perpendicular to the main foliation of a graphite-rich micaschist; PPL, sample PCM-47. (b) Garnet showing a pattern of inclusions of quartz and opaque minerals concordant to the main foliation of a micaschist with staurolite; PPL, sample PCM-651. (c) Garnet displaying a pattern of dendritic growth (very high growth velocity), with quartz inclusions concordant to the main foliation of a quartz micaschist; PPL, sample PCM-700. (d) Snow-ball garnet, showing sigmoidal inclusions of quartz in a micaschist with fibrolitic sillimanite; PPL, sample PCM-971. (e) Optically sector-zoned garnet porphyroblasts in a quartz micaschist showing compositional mica- and quartz-rich bands; XPL (left) – PPL (right), sample PCM-618. (f) Sector-zoned garnet with radial quartz inclusions in quartz micaschist with staurolite; XPL, sample PCM-702.

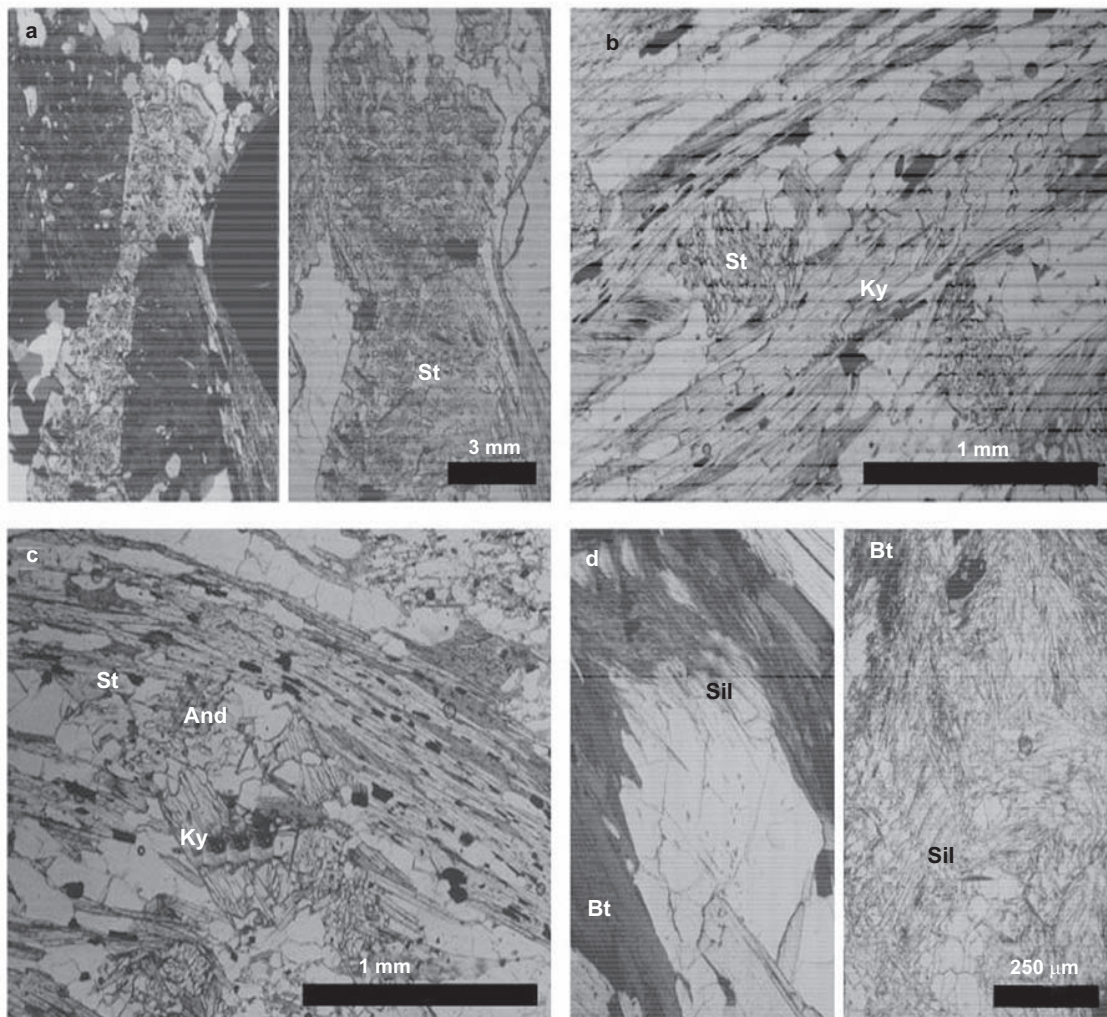


**Figure 5.** Petrographic features of the aluminosilicate phase-bearing pelitic rocks of the Silgará Formation at the CSM. (a) Staurolite porphyroblasts displaying penetration twinning and containing inclusions of quartz, graphite and opaque minerals discordantly with the external schistosity of the rock; XPL (left) – PPL (right), sample PCM-702. (b) Paragenesis staurolite-kyanite. Kyanite contains discordant quartz inclusions and staurolite shows rotational character; PPL, sample PCM-21. (c) Paragenesis staurolite-kyanite-andalusite; PPL, sample PCM-21. (d) Aggregates of fibrolitic sillimanite after biotite (left, PPL, sample PCM-981) and prismatic sillimanite (right, PPL, sample PCM-972).

of garnet is shown in Table 3. MgO contents in the garnets in the pelitic schists vary between 5.64 and 15.03, the content of FeO varies between 68.91 and 93.38, the content of MnO varies between 0.05 and 15.76 and the content of CaO varies between 1.00 and 10.92. Chemical zoning of garnet from the Silgará pelitic schists is illustrated in Mg-Mn-Fe and Ca-Mn-(Fe+Mg) triangular diagrams (Figure 7) and

X-ray element maps (Figure 8), which is summarized as follows: (1) garnet is almost pure almandine end member, with very low content of Mg, Mn and Ca. In addition, only a slight increase of Mn was observed at the core (e.g., PCM-700); (2) garnets exhibits normal zoning with increasing Mg and Fe components from core to rim and decreasing Mn and Ca components from core to rim, suggesting prograde metamorphism

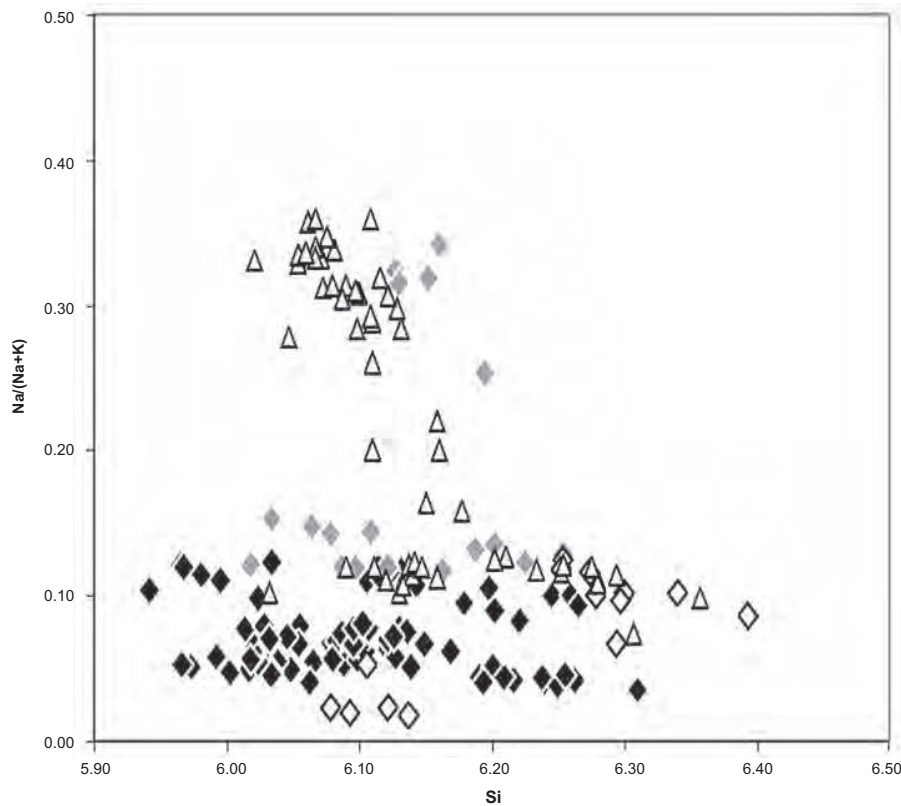


**Figure 6.** Chemical compositions of muscovite from pelitic rocks of the Silgará Formation at the CSM expressed in a Na/(Na+K) vs Si diagram; black, open and grey rombs indicate the mineral assemblages  $Sil \pm St \pm Grt$ ,  $St + And \pm Ky$  and  $St + Grt$ , respectively; the paragenesis  $And + Ky + Sil$  is indicated by open triangles

e.g., PCM-651, PCM-701, PCM-971); (3) garnet exhibits normal zoning through to the inner rim, but in the outer rim the chemical zoning is reversed, reflecting the effects of retrograde metamorphism (e.g., PCM-47, PCM-953); (4) sector-zoned garnet, with very different models of zoning even in thin section-scale (e.g., PCM-618). In some cases, distribution of elements follows a radial (sector) trend PCM-618, but in other cases distribution follows a patchy or concentric trend PCM-618, PCM-701 and PCM-702.

Staurolite shows pleochroism (x: dark yellow, y: light yellow, z: pale yellow), and occurs as porphyroblasts, from idioblastic to relictic character. It usually contains abundant inclusions of quartz and minor inclusions of graphite and opaque minerals. These inclusions are usually randomly oriented, but in some cases may be concordant or discordant with the main

schistosity of the rock. Rims of staurolite are straight or corroded by quartz and shapes range from rounded to elongated and locally overgrowth the main schistosity of the rock, suggesting a rotational and deformational event. Staurolite is partly replaced by white mica and chlorite at the rims and along cracks. In some samples staurolite exhibits replacement at the rims by fibrolite. The mineral chemistry of staurolite is shown in Table 4. Figure 9 illustrates color maps of staurolite, which exhibits a high-Fe content ( $X_{Fe} = 0.68-0.89$ ), but does not show any zonation in Fe and Mg (Figure 9a and 9b). Figure 9c shows a typical staurolite-kyanite grade pelite (PCM-905). Sample PCM-49 has the highest ZnO content (3.70 weight %) and homogeneous Zn distribution.

$Al_2SiO_5$  polymorphs. Kyanite occurs as discrete crystals, with porphyroblastic and poikiloblastic character. It is usually colorless and is closely associ-

ated with sillimanite (fibrolite) and andalusite. Andalusite occurs as discrete crystals with porphyroblastic and poikiloblastic character. It is usually very light pink or colourless and occurs as rectangular or rounded crystals. Sillimanite occurs as fibrolite, and the fibrous aggregate are folded. Usually it is interlayered, replacing biotite and white mica. It is also found at the rim of staurolite as a replacement. Very small fibers occur as inclusions in quartz, plagioclase and micas. The mineral chemistry of  $Al_2SiO_5$  polymorphs is shown in Table 5. In general, kyanite, andalusite and sillimanite do not display any variation in chemical composition. However, Fe in sillimanite is lower than Fe in andalusite and kyanite.

Plagioclase occurs in the granoblastic bands together with quartz, and shows a range of grain sizes, irregular and variable grain shapes, curved and irregular boundaries. A second type of plagioclase shows a xenoblastic to subidioblastic character, occasionally idioblastic character, is twinned or untwinned, and occurs also as porphyroblasts in augen structure, usually concordant with  $S_c$ , although sometimes is possi-

ble to find rotated porphyroblasts suggesting pre or syn-tectonic growth. Random and oriented inclusions of quartz, white mica, biotite and opaque minerals also occur. These two types of plagioclase exhibit a moderate replacement by sericite. A third type of plagioclase shows a xenoblastic character, variable to rounded shapes and small sizes, and occurs as inclusions generally in garnet. The mineral chemistry of plagioclase is shown in Table 6. The anorthite content of plagioclase in pelitic schists varies from 0.03 to 0.61. There are no clear relationships between the anorthite contents and the mineral assemblages. The highest  $X_{An}$  (0.61) was found in sample PCM-21 and the lowest (0.03) in sample PCM-701. Plagioclase from sample PCM-953 exhibits compositional Ca zoning from core ( $An_{15.34}$ ) to rim ( $An_{13.55}$ ), concordantly with the decrease of Ca in garnet from core to rim in the same sample.

**Accessory phases.** Epidote occurs as discrete crystal or aggregates of small and elongated prismatic crystals with subidioblastic to xenoblastic character. Distribution and orientation are random. It

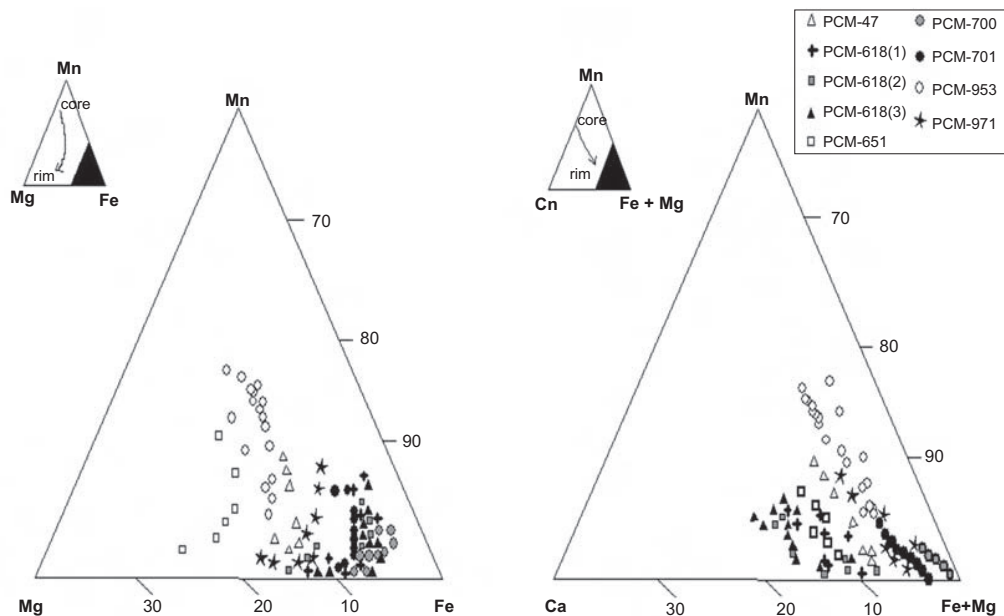


**Figure 7.** Chemical compositions of garnet from metapelites of the Silgará Formation at the CSM expressed in Mg-Mn-Fe and Ca-Mn-(Fe+Mg) diagrams.

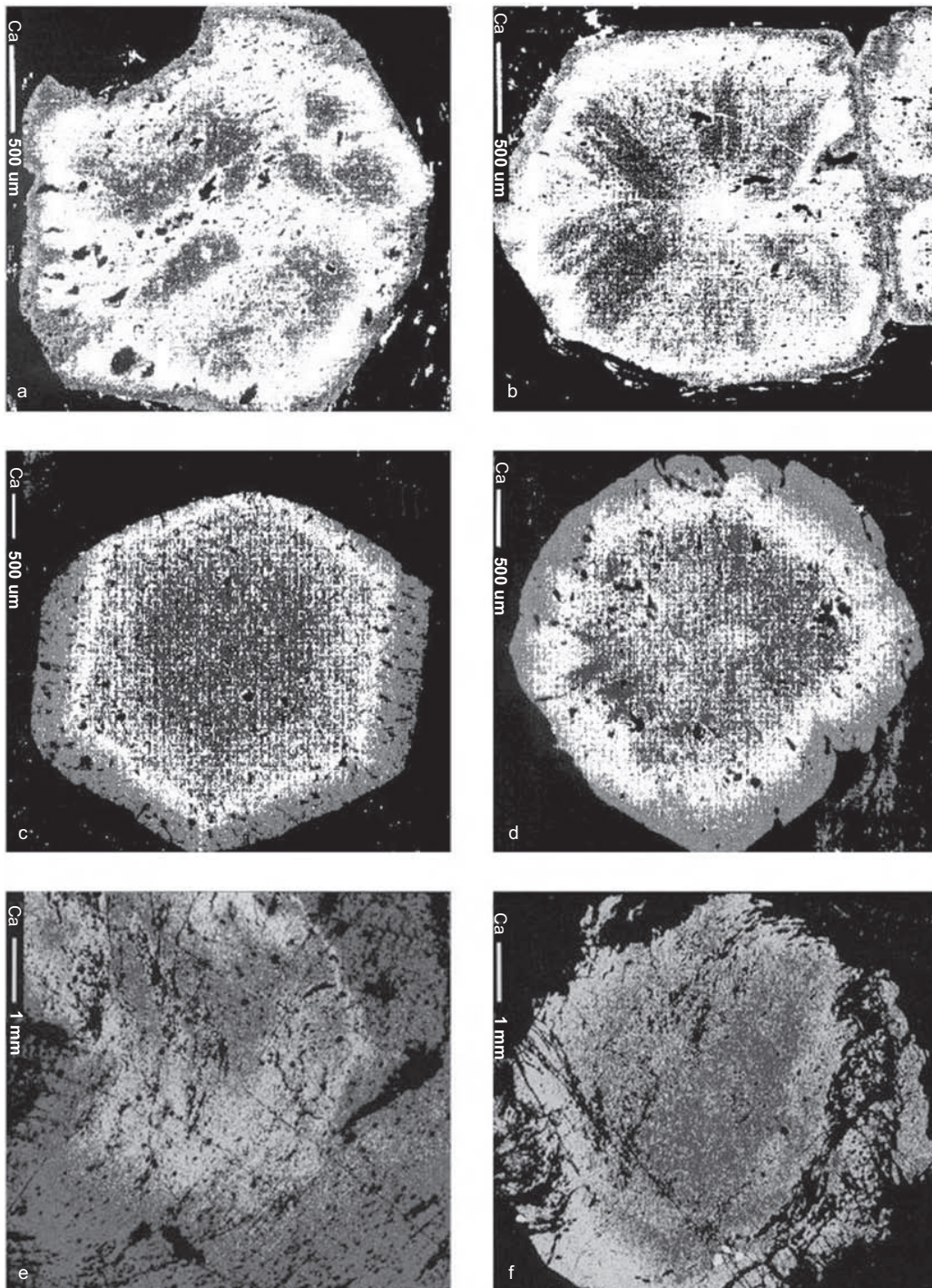


**Figure 8.** X-ray element maps for Ca of garnet porphyroblasts from metapelites of the Silgará Formation at the CSM. (a) PCM-618, sector-zoned garnet with patch zoning. (b) PCM-618, sector-zoned garnet with radial zoning. (c) PCM-702, euhedral garnet with a hexagonal concentric zoning. (d) PCM-701, subhedral garnet with radial and concentric zoning. (e) PCM-971, sigmoidal garnet showing an irregular concentric zoning. (f) PCM-971, sigmoidal garnet showing an irregular concentric zoning.

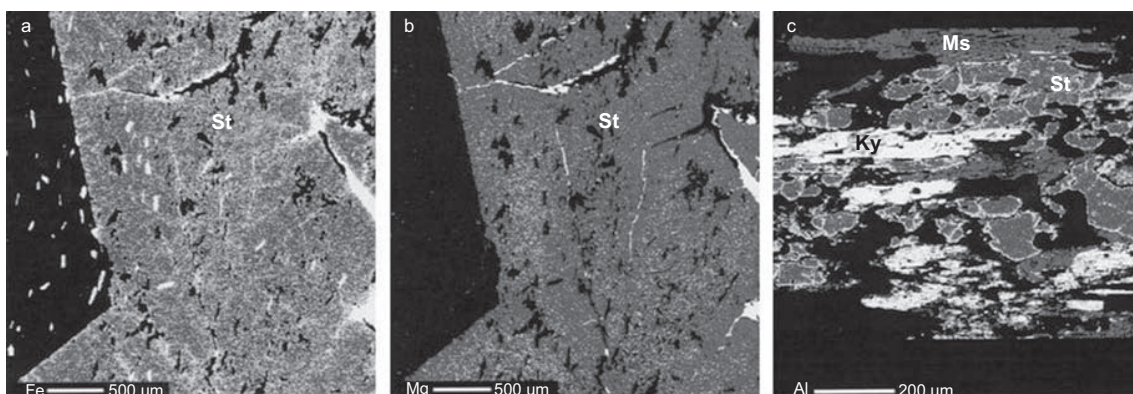


**Figure 9.** X-ray element maps of staurolite from metapelites of the Silgará Formation at the CSM. (a) and (b) PCM-701, staurolite porphyroblasts developing penetrating twinning and a nearly homogeneous distribution of Fe and Mg. (c) Staurolite associated to kyanite and muscovite, showing a different Al concentration.

shows a pleochroism (x: colorless, y: light yellow, z: light green), and some crystals exhibit optical zoning. Tourmaline occurs as discrete grains of subidioblastic and prismatic character, green to violet, and exhibits typical optical zoning and pleochroism. It is randomly oriented. It occurs in the matrix and as inclusions in major minerals. Apatite occurs as discrete and very small grains. It is subidioblastic and prismatic in shape and occurs in the matrix and as inclusions in quartz, plagioclase and micas. Zircon occurs in the matrix with random orientation as very small discrete grains. It is elliptical in shape and shows typical birefringence colors. Opaque minerals occur as discrete grains that show very different shapes and orientations both as a matrix phase and as inclusions in almost all major minerals. Rutile occurs as discrete randomly-oriented xenoblastic crystals and as matrix and inclusion phases. It is dark-yellow in color and has black haloes at the rims. Ilmenite forms discrete crystals with tabular habit, black in color, homogeneous distribution, and concordant to discordant orientation. Graphite appears as aggregates of very-fine flaky crystals, black in color, giving to the rock a clouded appearance.

### Metamorphism

Determination of metamorphic grade of the pelitic sequence of the Silgará Formation at the CSM is based on the experimentally defined stability of in-

dex minerals as well as on their chemical composition. Mineral assemblages, their relationships, structural features and mode of occurrence as well as common local alternation of lithological members with gradual transition suggest the existence of a volcanoclastic sedimentary sequence made of pelitic rocks with intercalations of semipelitic, psammitic, basic and carbonaceous rocks. Field and petrological studies show that the metamorphism of the Silgará Formation is characterized by the presence of typical index minerals of Barrovian type metamorphism (Miyashiro, 1994). On the basis of mineral assemblages in pelitic rocks, the Silgará Formation can be divided into a Barrovian-type facies series of biotite, garnet, staurolite-kyanite and sillimanite zones. A separation between the kyanite and staurolite zones has not been done in this study in spite of the occurrence of ductile shear zones with hydrothermal kyanite-bearing quartz veins. All pelitic schists contain the mineral assemblage quartz + plagioclase + biotite + muscovite, which is associated with sillimanite in the southwestern sector of the study area, where schists with garnet (PCM-953) and garnet + staurolite (PCM-971) assemblages also occur. Mineral assemblages containing aluminosilicates are characteristic in the northern part of the area. The three  $Al_2SiO_5$  polymorphs were observed in each one of the samples PCM-18, PCM-20 and PCM-21. The mineral assemblage quartz + plagioclase + biotite + muscovite + garnet + staurolite is distributed in the northern part

of the study area. The coexistence of biotite and muscovite, accompanied by quartz and plagioclase may be generated by a reaction at P-T conditions slightly below 400 °C and 4 kbar. The presence of garnet coexisting with biotite takes place below 500 °C. This idea is consistent with that of Spear (1993) where below 500 °C garnet occurs only in rocks with high Ca + Mn contents. For the mineral assemblage quartz + plagioclase + biotite + muscovite + garnet + staurolite, the reaction  $\text{Grt} + \text{Chl} = \text{St} + \text{Bt}$  reaches P-T temperatures 550 °C and pressure ranges from 4 to 6 kbar (Spear, 1993). The first appearance of kyanite can be related to its intergrowth with staurolite, which is due to the close relationship between the structures of these minerals. Therefore, the mineral assemblage quartz + plagioclase + biotite + muscovite + staurolite + kyanite may establish the highest pressure range 6-7 kbar at about 600°C for the Silgará Formation at the CSM. Resorption and replacement of kyanite by sillimanite suggests a probable decrease in pressure (close to 600°C). Andalusite is present in the mineral assemblages  $\text{Qtz} + \text{Pl} + \text{Bt} + \text{Ms} + (\text{Ky} + \text{And})$  or  $+(\text{Ky} + \text{And} + \text{St})$  or  $+(\text{St} + \text{And})$ . The reaction kyanite = andalusite occurs at the retrograde stage of metamorphism during a decrease of both P-T or only P. According to Goldsmith et al. (1971) the metamorphism of the Silgará Formation may have occurred during the 410-450 Ma event. The metapelitic sequence is not always complete, because in some cases the lower-grade metamorphic zones do not occur. A complex tectonic history probably played a very important role in breaking the metamorphic zoning and therefore some apparent isograds may correspond to faults. On the other hand, the authors consider that is still unclear how the late emplacement of orthogneiss masses affected the metapelitic sequence, as well as the occurrence of crustal granitoid rocks that are generally form to contact aureoles, taking into account that in sectors such as La Laguna, textural evidence may indicate the occurrence of hornfelsic rocks and mineral assemblages that overprinted to early mineral phases and fabrics. In the contact between the Silgará Formation and the Bucaramanga Gneiss Complex, the contact is often defined by the biotite-sillimanite isograd

(Ward et al., 1973; Restrepo-Pace et al., 1997), though this differentiation method seems to imply a common metamorphism for both units (Ordoñez-Carmona *et al.*, 2006).

## Geothermobarometry

Figures 10 and 11 summarize the estimated P-T conditions of evolution for the Silgará Formation metapelitic rocks at the CSM. The thermobarometric estimates were done in domains of samples showing textural and chemical evidence of equilibrium among the phases under consideration. Mineral compositions were used with the computer program GTB (Spear & Kohn, 2001), which incorporate most published geothermobarometers, to obtain equilibrium pressures and temperatures from garnet bearing assemblages. Various assemblages were used to calculate pressures and the garnet-biotite assemblage was used to calculate temperatures. Temperatures and pressures for 3 representative samples (PCM-618, PCM-953 and PCM-971) were calculated using the garnet-biotite geothermometer and the garnet-plagioclase-biotite-muscovite, GASP and garnet-muscovite-biotite-SiAl<sub>2</sub>O<sub>5</sub> geobarometers. Sample PCM-618 consists of sector-zoned and poikiloblastic porphyroblasts of garnet in a granolepidoblastic matrix of quartz, plagioclase, biotite and muscovite. Plagioclase also occurs as inclusion in poikiloblastic garnet. Sample PCM-953 consists of porphyroblastic garnet in a granolepidoblastic matrix of quartz, plagioclase, muscovite, biotite and sillimanite. Sample PCM-971 consists of porphyroblastic garnets in a granolepidoblastic matrix of quartz, biotite and muscovite. Chemical compositions were taken from the rim of different sectors of the garnets, which show moderate to strong chemical zoning, and from the rims of plagioclase, biotite and muscovite crystals, which do not show strong or systematic chemical zoning. All iron in biotite and garnet was assumed to be Fe<sup>2+</sup>.

Metamorphic temperatures were estimated using Fe-Mg exchange among minerals according to: (1) Ganguly & Saxena (1984), (2) Perchuk & Lavrent'eva (1984), (3) Indares & Martignole (1985), (4) Ferry & Spear with Berman (1990), (5)

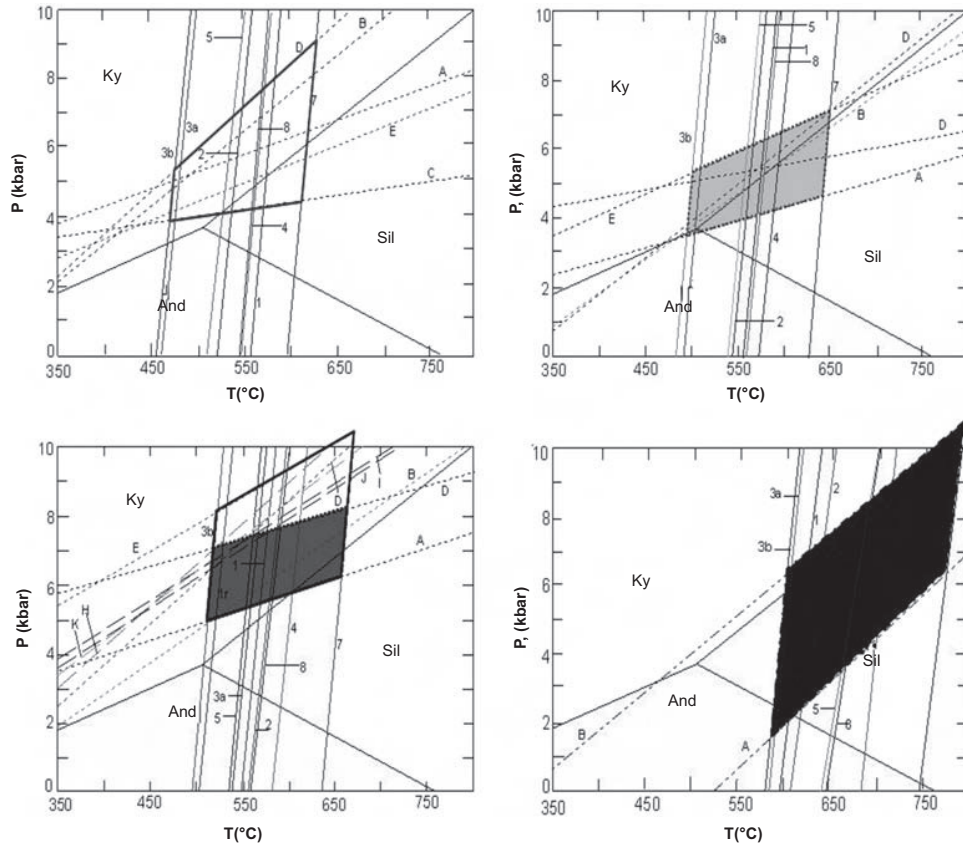


**Figure 10.** P-T estimates using different calibrations of geothermobarometers from GTB program by Spear and Kohn (2001): Grt-Bt thermometer and (a) Grt-Pl-Bt-Ms barometer from sample PCM-618, sector-zoned garnet, (b) Grt-Pl-Bt-Ms barometer from sample PCM-618, poikiloblastic garnets, (c) Grt-Pl-Bt-Ms and GASP barometers from sample PCM-953, (d) Grt-Ms-Bt-Al<sub>2</sub>SiO<sub>5</sub> barometer from sample PCM-971. Triple point for aluminosilicates after Holdaway (1971).

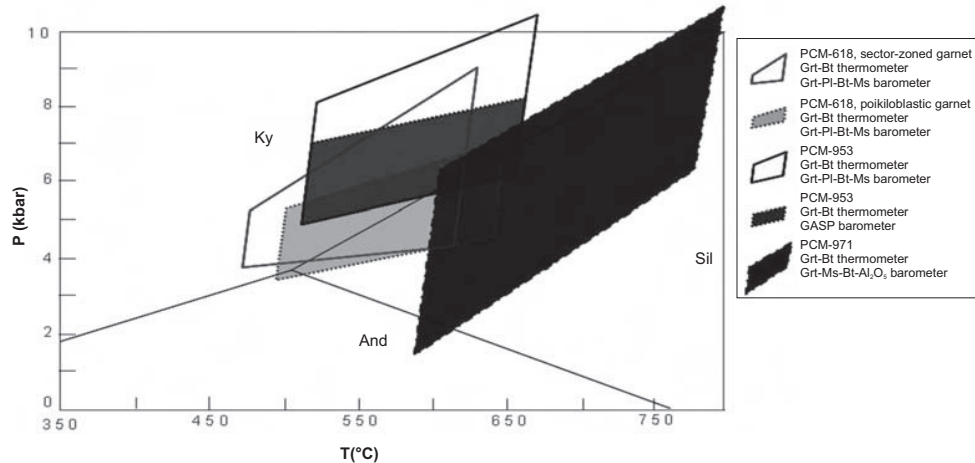


**Figure 11.** P-T diagram showing polygons of total ranges of calculated temperatures and pressures from pelites of the Silgará Formation at the CSM, using different calibrations of geothermobarometers from GTB program by Spear and Kohn (2001). Triple point for aluminosilicates after Holdaway (1971).

Patino Douce *et al.* (1993), (6) Holdaway *et al.* (1997), (7) Gessmann *et al.*, (1997), (8) Kleemann & Reinhardt (1994). Metamorphic pressures were estimated as follows: for samples PCM-618 and PCM-953 using the Grt-Pla-Bt-Ms barometer of (A) Ghent & Stout (1981) Fe end member, (B) Hodges & Crowley (1985), (C) Powell & Holland (1984) with Hodges & Spear (1982), (D) Hoisch (1990) Fe end member, (E) Hoisch (1990) Mg end member; for sample PCM-953 using the GASP barometer of (A) Newton & Haselton (1981), (B) Hodges & Spear (1982), (C) Ganguly & Saxena (1984), (D) Hodges & Crowley (1985); for sample PCM-971 using the Grt-Ms-Bt-Al<sub>2</sub>O<sub>5</sub> barometer of (A) Hodges & Crowley (1985), (B) Holdaway *et al.*, (1988). According to geothermobarometric calculations reported in this study, temperature and pressure conditions for this area are 400-600 °C and 4.0-6.5 kbars, respectively.

\*references as listed in the GTB Geothermobarometry software of Spear & Kohn (2001).

### Reaction history and P-T paths

Figure 12 illustrates the P-T trajectories postulated in this study for the Silgará Formation pelites at the CSM from mineral assemblages, their textural relations and mineral compositions, which can be compared with the P-T path proposed by García *et al.*, (2005) for these rocks and two different model P-T paths by Spear (1993) followed by low-Al pelites for typical regions have undergone crustal thickening or contact metamorphism. The P-T conditions estimated by geothermobarometry were verified by constructing a petrogenetic grid that constrains the mineral stability fields and reactions known with various

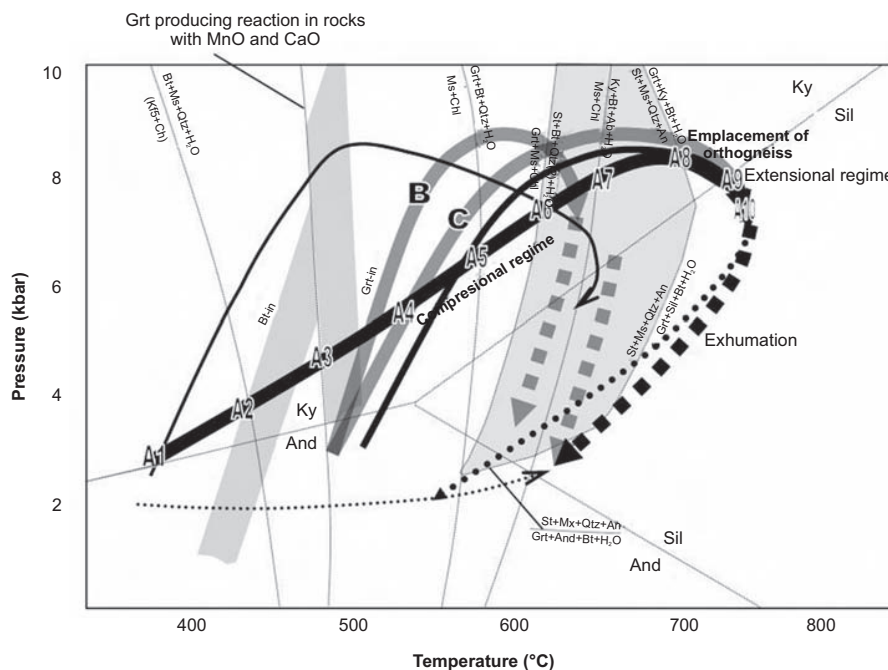
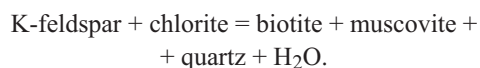


**Figure 12.** Petrogenetic grid illustrating mineral reactions in pelites as a function of pressure and temperature. Model of metamorphic P-T evolution followed by the Silgará Formation pelites at the CSM (black- and grey-thick arrows), compared with the P-T path proposed by García *et al.*, (2005) indicated by a black arrow, and two P-T paths (Spear, 1993) for typical regions that have undergone Barrovian facies metamorphism (thin continuous-black arrow) or contact (thin dotted-black arrow) metamorphism. The Al<sub>2</sub>SiO<sub>5</sub> triple point after Holdaway (1971). The narrow grey areas correspond to the biotite- and garnet-in reaction after Yardley (1989), and the wide grey area shows the stability field of staurolite after Bucher & Frey (1994).

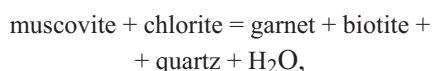
degrees of certainty, which can be used to decipher the reaction history of the investigated rocks.

The path **A1-A10** starts out at c. 350°C and 2 kbar. However, the P-T paths B and C at the one proposed by García *et al.* (2005) correspond to the P-T evolution of garnet-bearing pelites that reached the staurolite-kyanite or sillimanite conditions, and probably start out at the same conditions (c. 480-500 °C and 2 kbar), but follow slightly different trajectories. Our model can be summarized as follows: a given volume of rock experienced gradual crustal shortening and thickening, accompanied by an increment of pressure and temperature conditions, as a result of burial until reaching the maximum pressure condition ( $P_{\text{peak}}$ ) is reached. The thickened crust is uplifted slowly and erosion tends to restore the original crust, which is characterized by decompression, with a continued increasing temperature until to reach the maximum temperature condition ( $T_{\text{peak}}$ ). Then, the volume of crust experienced progressive crustal uplifting, accompanied by erosion, rehydration, cooling and decompression.

**Biotite-in reaction.** At **A1**, the initial assemblage in low-Al pelites was probably chlorite + K-feldspar (+ muscovite + quartz), from which biotite formed at 380 °C and 3.8 kbar (**A2**) by the continuous reaction



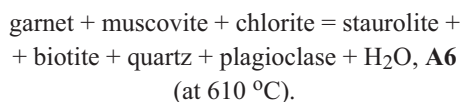
**Garnet-in reaction.** The garnet isograd reaction (**A3**) is strongly dependent on bulk rock composition and specially MnO and CaO content (Spear, 1993). In MnO- and CaO-rich rocks, garnet may appear at temperatures below 450 °C whereas in MnO- and CaO-poor rocks, garnet may not appear to well above 500 °C (Spear, 1993). Therefore, at **A4** garnet is probably present because of the MnO content of most pelites. No discontinuous reaction has been encountered up to  $\approx 530$  °C (**A5**), when garnet was produced by the continuous reaction



which explains a simultaneous decrease in muscovite and chlorite and increase in biotite contents

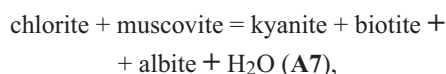
within the garnet zone, compared with the lowest-grade pelites from the biotite zone. The garnet zone is characterized by the mineral assemblage garnet + chlorite + biotite + muscovite + quartz, which is stable over an interval of metamorphic grade above the garnet-in isograd.

**Staurolite-in reaction.** At the staurolite isograd, the first appearance of staurolite may be related to biotite-producing and chlorite- and muscovite-consuming reactions, because the staurolite zone is marked by a strong increase in the modal abundance of biotite at the expense of chlorite and muscovite. Textural evidence shows that staurolite may be produced by a garnet-consuming discontinuous reaction, such as

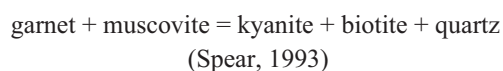


When this reaction has finished some more staurolite may be produced by a garnet-absent continuous reaction involving the remaining phases.

**Kyanite-in reaction.** The staurolite zone corresponds to buffering along this reaction to the intersection where chlorite, biotite, garnet, staurolite and kyanite coexist (Lang and Rice, 1985). The kyanite + staurolite association suggests that kyanite and staurolite crystallized from an appropriate bulk composition in the appropriate P/T range (Şahin and Erkan, 1994). According to Lang and Rice (1985), the net reaction at the intersection is approximated by the transition zone reaction

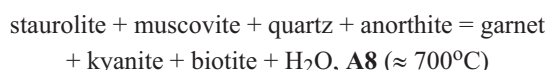


which explains the probable kyanite-forming reaction developed through a chlorite-consuming reaction. However, kyanite may also be formed during a garnet-consuming reaction such as

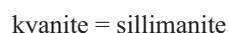
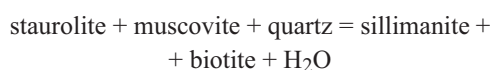
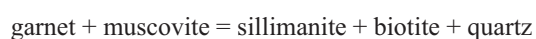
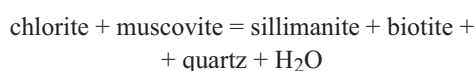


The pelites from the structurally upper level of the kyanite zone are characterized by the mineral as-

semblage kyanite ± staurolite + biotite + muscovite + plagioclase + quartz. With increasing temperature, staurolite becomes unstable and reacts to produce garnet, kyanite and biotite. Staurolite disappears at the kyanite isograd as a result of the discontinuous reaction



**Sillimanite-in reaction.** According to Zhao & Cawood (1999) the following sillimanite-producing reactions may be considered:



Textural evidence from the Silgará Formation pelites suggests that the production of sillimanite includes the appearance of fibrolitic sillimanite-biotite intergrowths with the consumption of chlorite and muscovite or pseudomorphs after garnet porphyroblasts, fibrolite at the expense of staurolite porphyroblasts, with or without the production of garnet, relict kyanite within muscovite crystals, and the polymorphic reaction kyanite = sillimanite (**A9**). Chemical zoning and sillimanite inclusions in muscovite and quartz may indicate decrease in pressure after the formation of sillimanite during staurolite-consuming reactions (increasing temperature). After a near isothermal decompression, the final assemblage will be garnet + staurolite + sillimanite + biotite (+ muscovite + quartz), **A10**.

Up to this point, the Silgará Formation pelites have undergone medium-P/high-T conditions of Barrovian facies metamorphism, corresponding to the Ky-Sil series of Miyashiro (1994), following a clockwise pressure-temperature path, which is char-

acteristic for the metamorphic evolution of most orogenic belts (Brown, 1993).

The final event described in this study is a retrograde metamorphic event, characterized by a decrease in both temperature and pressure parameters. The retrogressive reactions are related to partial replacement of garnet by chlorite and/or biotite along cracks, heavily corroded staurolite enclosed by sericite and chlorite, replacement of biotite by chlorite or ilmenite exsolution in biotite. However, the retrograde trajectory in the Silgará Formation pelites is not well constrained and can only be inferred from mineral assemblages belonging to greenschist facies. The coexistence of kyanite-sillimanite-andalusite in staurolite-bearing rocks, mineral assemblages and textural observations indicate a sequence of occurrence: first coexistence of kyanite and staurolite, followed by breakdown of kyanite and with presence of sillimanite, and lastly a retrograde metamorphism with the occurrence of andalusite after kyanite. However, the presence of the three  $\text{Al}_2\text{SiO}_5$  polymorphs in some samples suggests a more complex P-T metamorphic evolution. Therefore, we propose the occurrence of alternative P-T paths recorded by the Silgará pelites from the garnet (**B**) and staurolite-kyanite (**C**) metamorphic zones. The alternative P-T paths take into account strong textural evidence supporting the first appearance of kyanite “kyanite-in isograd” by the polymorphic reaction  $\text{And} = \text{Ky}$ . However, the P-T trajectory **B** corresponds to pelites evolved from the garnet to the staurolite-kyanite stability fields, without production of sillimanite, and the P-T trajectory **C** closest to the triple point should be considered with the following reaction sequence andalusite ® kyanite ® sillimanite based on pelites that reached the sillimanite conditions.

## Discussion

A main characteristic of orogens is a complex deformation history involving various tectonic processes such as burial of crustal slices followed by exhumation of deep metamorphic rocks by nappe stacking, syn-orogenic to post-orogenic extension and tectonic denudation (Duguet *et al.*, 2007). Therefore, the re-

construction of a P-T path is sometimes difficult to constrain. However, this problem can be overcome when the metamorphic series contain garnet-bearing metapelitic rocks such as those of the Silgará Formation, which underwent metamorphism with a peak at the upper amphibolite facies conditions, being affected during the last stage of deformation by the emplacement of syn-tectonic intrusions (Orthogneiss). Campos (1999) reported that the occurrence of veins mainly composed of quartz with minor calcite in metasomatic zones of the Silgará Formation metacarbonate rocks indicates a remobilization of SiO<sub>2</sub> and CaO due to the action of late magmatic fluids associated to the emplacement of the Orthogneiss protolith, which circulated along tectonic discontinuities. Additional evidence on the external fluid contribution derived from syn-metamorphic intrusions corresponds to the development of a H<sub>2</sub>O-rich diopside reaction zone in the presence or absence of scapolite in the metasomatic rocks of the Silgará Formation. Finally, a thermal event overprinted to the regional metamorphism of the Silgará Formation which the authors propose as due to the emplacement of calc-alkaline granitoids of Triassic-Jurassic age, that are generally found to contact aureoles, and for example in sectors such as La Laguna, textural evidence indicates the occurrence of poikiloblastic andalusite in hornfelsic rocks, with mineral assemblages overprinting early mineral phases and fabrics. During a Late Triassic-Early Jurassic intrusive-related regional metamorphic episode, high-T and low-P conditions of the Santander Massif prevailed (Restrepo-Pace, 1995). The reconstruction of the P-T paths experienced by this metamorphic unit is a crucial point to decipher the tectonic setting of the deformation events and any proposed model should take into account thermobarometric data. However, the geodynamics and tectonic setting of the Santander Massif are still matter of debate.

### *P-T paths*

García *et al.* (2005) already documented P-T conditions for the Silgará Formation at the CSM (6.1-8.5 kbar and 616-784 °C). Our results are consistent with a two-stage tectonothermal evolution under

high-grade conditions: (1) an early compressional phase of deformation that led to upper amphibolite facies Barrovian-type metamorphism and (2) a subsequent extensional phase of deformation that led to near-isothermal decompression and the emplacement of orthogneiss masses. A final Evidence of stage of near-isobaric cooling to greenschist facies conditions is widespread. Both prograde and retrograde metamorphic evolution may be constrained and characterised by initial crustal shortening and thickening associated with thrusting, subsequent slow exhumation and final cooling. However, due to the preservation of prograde mineral assemblages and critical reaction textures, a more complex series of P-T paths can be inferred. The tectono-metamorphic history of the Silgará Formation metapelites is characterised by clockwise P-T trajectories (Figure 9). The inferred P-T paths are interpreted to result from one geological event, but during different stages of deformation. However, this assumption must be tested by geochronological data.

### *Tectonic implications*

Based in both petrological evidence and the inferred P-T paths for the Silgará Formation pelites, we postulate two possible tectonic scenarios in which the metamorphism of this geological unit might have taken place: (1) medium-grade metamorphism related to collision tectonics and subsequent decompression from extensional collapse of the tectonically thickened crust, probably accompanied by the emplacement of syn-metamorphic intrusions (Orthogneiss) and (2) overprinted thermal metamorphism related to the emplacement of calc-alkaline granitoids of Triassic-Jurassic age. The shape and direction of the clockwise P-T paths inferred in the current study support these interpretations. Subsequent decompression and uplift of the pelites, initially under medium-pressure conditions, can be related to an extensional collapse of the thickened crust, where the emplacement of orthogneiss masses provided further heat input into the pelites during their last stage of deformation. Later cooling of the pelites can be related to cooling of the orthogneiss masses. Restrepo-Pace (1995) report a U/Pb zircon age of 480 Ma for the

emplacement of syn-tectonic intrusives suggesting a magmatic event in the late Ordovician or early Silurian. Therefore, the age of the orthogneiss emplacement must be similar to that of the Silgará Formation, which can be explained only if the emplacement and metamorphism processes of orthogneiss masses occurred at the beginning of the last stage of deformation that affected the Silgará Formation pelites.

### ***Uplift and exhumation***

The thickened crust represented by the medium-pressure, high temperature metapelites of the Silgará Formation was uplifted slowly and erosion led to restore the original crust, which is characterized by decompression. During this stage the emplacement of orthogneiss masses probably occurred. However, as initial uplift rates are slow compared with heat transport rates, these metapelites were affected by a continuously increasing temperature during uplift until they reached the thermal peak, after which these rocks experienced cooling, accompanied by retrograde metamorphism documented by generally incomplete rehydration reactions and least not-hydrated mineral phases have been preserved as relicts. The uplift of deeply buried rocks in subduction or collision zones can be explained by the buoyancy of crustal rocks at depth (von Blanckenburg & Davies, 1995; Ernst *et al.*, 1997): (1) the buoyancy of tectonically thickened crust when material is removed from the upper crust by erosion or faulting or (2) break-off of the subducting slab, thus removing slab pull and allowing the subducting crust to return buoyantly to the surface. Exhumation of the Silgará Formation is represented by the return toward the Earth's surface of the deeply buried pelitic rocks, a process that is generally driven either by erosion or low-angle normal faulting or both; ductile extension of the crust or lithosphere is slow and cannot account for more than a small fraction of exhumation (Ring *et al.*, 1999).

### **Conclusions**

The sequence of mineral assemblages, metamorphic reaction history and estimated clockwise P-T path for

the Silgará Formation at the CSM let us to constrain its tectono-metamorphic evolution, which is characterized by initial crustal shortening and thickening associated with thrusting, subsequent slow exhumation and final cooling, which is characteristic during continental collision (Brown, 1993). Petrographic observation and thermobarometric data indicate that the investigated pelites underwent regional prograde metamorphism and the metamorphic zones equilibrated at significantly different peak pressures and temperatures along the kyanite geotherm. According to the metamorphic reactions and the P-T evolution model proposed in this study, the first mineral assemblage observed was biotite + muscovite + quartz, which probably formed near 425°C and 3.8 kbar. The coexistence of garnet in mineral assemblages with biotite occurs approximately at 475°C and 4.7 kbar. Conditions for the first appearance of staurolite are close to those for the first appearance of kyanite, reaching probably the peak of pressure, 625°C and 7.5 kbar and 650°C and 8.0 kbar, respectively. Kyanite breakdown into sillimanite and the peak temperature were estimated at around 680°C and 8.0 kbar, which however do not correspond to the peak temperature (740°C and 7.0 kbar). The Silgará Formation pelites exhibit a retrograde metamorphism with the occurrence of andalusite and accompanied by reverse zoning at the outer rim of garnets, and chloritization and sericitization processes. Calculations for sample PCM-953 were carried out using data from the contact between the rims of garnet and biotite, yielding a temperature range of 497-583°C according to different calibrations of the garnet-biotite pair. This temperature could be interpreted as the peak of the retrograde metamorphic event. There is a strong evidence on the occurrence of an overprinted thermal event to the regional metamorphism. The uncertainties of the P-T data are related to the variability of mineral compositions within the studied rocks and to the lack of control of thermodynamic parameters. However, a general trend toward medium pressures at low temperatures of metamorphism is clearly shown by the observed mineral associations. The P-T paths appear to favour models involving the delamination of lithospheric mantle as a factor con-

tributing to the change from compressional to extensional tectonics at the CSM. Medium-pressure pelitic rocks of the Silgará Formation were probably formed during a collision, with a buried crust reaching pressures up to 6.5 kbar, equivalent to 27 km depth, estimated for the kyanite-bearing pelites. Near-isothermal decompression commonly follows the crustal thickening and initially buried rocks were rapidly exhumed as the crust was thinned by structural collapse, extension and erosion. Therefore, the metamorphic evidence indicates such a buried crust as a consequence of its tectonic transport during a continental collision is the formation of middle-pressure kyanite-bearing pelites, followed by recrystallisation of lower pressure assemblages within a clockwise P-T. However, to confirm this hypothesis new field and petrological studies should be carried out and geochronological studies are necessary to constrain the P-T-t paths of the Caledonian Silgará pelites.

This work formed part of the MSc Thesis carried out by O. Castellanos at Shimane University (Japan). The authors are indebted to Universidad Industrial de Santander and Instituto Colombiano para el Desarrollo de la Ciencia y la Tecnología “Francisco José de Caldas” Colciencias through Grant No. 1102-05-083-95 financially supported fieldwork (Research Project: “Metamorphism and associated metallogeny of the Santander Massif, Eastern Cordillera, Colombian Andes”). We thank to Department of Geoscience of Shimane University. The authors are most grateful to the above-named people and institutions for support.

## References

- Banks, P., Vargas, R., Rodríguez, G.I., Shagam, R. (1985). Circón U-Pb ages from orthogneiss, Pamplona, Colombia. VI Cong. Latinoam. Geol. Bogotá. Resúmenes.
- Bence, A.E. and Albee, A.L. (1968). Empirical correction factors for the electron microanalysis of silicates and oxides. *Journal of Geology*, Vol. 76, pp. 382-403.
- Boinet, T., Bourgeois, J., Bellon, H., and Toussaint, J. (1985). Age et repartition du magmatisme pré-mésozoïque des Andes de Colombie. *Comptes rendus hebdomadaires des séances de L'Académie des Sciences. Serie D: Sciences Naturelles*, Vol. 300(II), 445-450.
- Brown, M. (1993). P-T-t evolution of orogenic belts and the causes of regional metamorphism. *Journal of the Geological Society, London* 150, 227-241.
- Bucher, K., Frey, M. (1994). *Petrogenesis of Metamorphic Rocks*. 6<sup>th</sup> edition Complete revision of Winkler's textbook, 318pp.
- Campos, N. (1999). Estudio Mineralógico y Petrográfico de las Metamorfitas al Occidente del Municipio de Mutiscua (Norte de Santander). Tesis de Pregrado, Universidad Industrial de Santander, Bucaramanga (Colombia).
- Cardona, A. (2003). Correlações entre fragmentos do embasamento Pré-Mesozoico da terminação setentrional dos Andes Colombianos, com base em dados isotópicos e geocronológicos. Dissertação de Mestrado, Universidade de São Paulo, Instituto de Geociências, 149 pp.
- Castellanos, O. (2001). Chemical composition of the rock-forming minerals in the Silgará formation and P-T conditions in the Mutiscua area, Santander Massif, Eastern Cordillera, Colombia. Unpublished Master Thesis, Shimane University, Matsue (Japan), 146 pp.
- Castellanos, O., Ríos, C., and Takasu, A. (2004). Chemically sector-zoned garnets in the metapelitic rocks of the Silgará Formation in the central Santander Massif, Colombian Andes: occurrence and growth history. *Boletín de Geología UIS*, Vol. 26, pp 91-18.
- Cooper, M.A., Addison, F.T., Álvarez, R., Coral, M., Graham, R.H., Hayward, A.B., Howe, S., Martínez, J., Naar, J., Peñas, R., Pulham, A.J. and Taborda, A. (1995). Basin development and tectonic history of the Llano Basin, Eastern Cordillera, and middle Magdalena Valley, Colom-

- bia, *Am. Assoc. Petrol. Geol. Bull.* 79, pp. 1421–1443.
- Deer, W. A., Howie, R. A. and Zussman, J. (1982). *An introduction to the rock-forming minerals*. Longman, New York, 696 p.
- Dörr, W., Grösser, J., Rodriguez, G., Kramm, U., 1995. Zircon U-Pb age of the Paramo Rico tonalite-granodiorite, Santander Massif (Cordillera Oriental, Colombia) and its geotectonic significance. *Journal of South American Earth Sciences* 8(2), 187-194.
- Duguet, M., Le Breton, N., and Faure, M. (2007). P-T paths reconstruction of a collisional event: The example of the Thiviers-Payzac Unit in the Variscan French Massif Central. *Lithos*, Vol. xx, pp. xxx–xxx
- Ernst, W.G., Maruyama, S. and Wallis, S. (1997). Buoyancy-driven, rapid exhumation of ultrahigh-pressure metamorphosed continental crust. *Proceedings of the National Academy of Sciences*, Vol. 94, pp. 9532–9537.
- Forero, A. (1990). The basement of the Eastern Cordillera, Colombia: An allochthonous terrain in northwestern South America. *Journal of South American Earth Sciences*, Vol. 3(23), pp. 141-151.
- García, C. and Ríos, C. (1998). Mineralogy and petrography of the metamorphic rocks to the west of Pamplona (Norte de Santander). Conference, XVI International Post-graduate Course in Metallogeny. Junio 9-21 de 1997, Quito, Ecuador.
- García, C. y Castellanos O. (1998). Petrografía de la Formación Silgará en la Cordillera Oriental, Colombia. X Congreso Latinoamericano de Geología, Buenos Aires, Argentina, Memorias, T.2, 263-268.
- García, C., y Ríos, C. (1999). Metamorfismo y metalogenia asociada del Macizo de Santander, Cordillera Oriental, Colombia. Informe final Proyecto de Investigación. Universidad Industrial de Santander - Colciencias, p.191.
- García, C., y Campos, N. (2000). Composición química y mineralogía de las biotitas metamórficas del sector central del Macizo de Santander, Colombia. *Boletín de Geología UIS*, Vol. 22 (37), 18-27.
- García, C., Ríos, C., and Castellanos, O. (2005). Medium-pressure metamorphism of the Silgará Formation in the central Santander Massif, Eastern Cordillera, Colombian Andes: constraints for a collision model. *Boletín de Geología UIS*, Vol. 27 (2), 43-68.
- Gélvez, J. and Márquez, R. (2002). Caracterización textural del granate y de sus elementos de deformación asociados, y modelamiento de su historia de nucleación y crecimiento en las rocas metapelíticas de la Formación Silgará en la región suroccidental del Macizo de Santander. Tesis de Pregrado, Universidad Industrial de Santander, Bucaramanga (Colombia).
- Goldsmith, R., Marvin, R., and Mehnert, H. (1971). Radiometric ages in the Santander Massif, eastern Cordillera, Colombian Andes. *U.S. Geological Survey Professional Paper*, Vol. 750-D, D41-D49.
- Gómez, S.I. y Ávila, G.A. (2006). Petrogénesis de las rocas calcosilicatadas que ocurren como bandas de reacción entre mármoles y rocas metapelíticas de la Formación Silgará, región Central del Macizo de Santander. Tesis de Pregrado, Universidad Industrial de Santander, Bucaramanga (Colombia).
- González de Juana, C., Iturralde, J., Picard, X. (1950). *Geología de Venezuela y de sus cuencas petrolíferas*: Ediciones Fonives, Caracas. Vol.1, 407 p.
- Kammer, A. (1993). Steeply dipping basement faults and associated structures of the Santander Massif, Eastern Cordillera, Colombian Andes. *Geología Colombiana*, Vol. 18, pp. 47-64.
- Kretz, R. (1983). Symbols for rock-forming minerals. *American Mineralogist*, Vol. 68, pp. 277-279.

- Holdaway, M. (1971). Stability of andalusite and the aluminum silicate phase diagrams. *American Journal of Science* 271, 97-131.
- Lang, H.M. and Rice, J.M. (1985). Regression Modelling of Metamorphic Reactions in Metapelites, Snow Peak, Northern Idaho. *Journal of Petrology* 26(4) 857-887.
- Mantilla, L., Ordoñez, J., Cepeda, S., and Ríos, C. (2001). Study of the paleofluids in the Silgará Formation and their relationship with deformation processes, Aratoca-Pescadero area (southwestern Santander Massif). *Boletín de Geología UIS*, Vol. 23(38), pp. 69-75. Mantilla, L., Ríos, C., and Castellanos, O. (2002). Study of the rehydration process of the Silgará Formation metamorphic rocks, from the compositional analysis of chlorite, southwestern Santander Massif. *Boletín de Geología UIS*, Vol. 24(39), pp. 7-17.
- Mantilla, L., Ríos, C., Gélvez, J., Márquez, R., Ordoñez, J., and Cepeda, S. (2003). New evidences on the presence of a shear band in the metapelitic sequence of the Silgará Formation, Aratoca-Pescadero area (southwestern Santander Massif). *Boletín de Geología UIS*, Vol. 25(40), pp. 81-89.
- Miyashiro, A. (1994). *Metamorphic Petrology*. Oxford University Press, U.K., 404p.
- Montenegro, G., y Barragán, M. (1999). *Metamorfismo y Evolución Metamórfica del área comprendida entre los municipios de Vetas (Santander) y Mutiscua (Norte de Santander)*. Tesis de Pregrado, Universidad Industrial de Santander, Bucaramanga (Colombia).
- Ordoñez, J. (2003). Petrology and geochemistry of the granitoids at the Santander Massif, Eastern Cordillera, Colombian Andes. Unpublished Master Tesis, Shimane University, Matsue (Japan), 150 pp.
- Ordoñez, J., and Mantilla, L. (2004). Significance of an early Cretaceous Rb-Sr age in the Pescadero Plutón, Santander Massif. *Boletín de Geología UIS*, Vol. 26 (43), pp. 115-126.
- Ordoñez-Carmona, O., Restrepo, J.J., and Martins, M. (2006). Geochronological and isotopic review of pre-Devonian crustal basement of the Colombian Andes. *Journal of South American Earth Sciences*, Vol. 21(4), pp. 372-382.
- Pennington, W.D. (1981). Subduction of the East Panama Basin and Seismotectonics of the northwestern South America, *J. Geophys. Res.*, Vol. 86(B11), pp. 10753-10770.
- Restrepo, J.J. and Toussaint, J.F. (1988). Terranes and continental accretion in the Colombian Andes, *Episodes* 11, pp. 189-193.
- Restrepo-Pace, P. (1995). Late Precambrian to Early Mesozoic tectonic evolution of the Colombian Andes, based on new geochronological, geochemical and isotopic data. Unpublished Ph.D Thesis, University of Arizona, 195 p.
- Restrepo-Pace, P., Ruiz, J., Gehrels, G., and Cosca, M. (1997). Geochronology and Nd isotopic data of Grenville-age rocks in the Colombian Andes: New constraints for late Proterozoic-early Paleozoic Palecontinental reconstruction of the Americas. *Earth and Planetary Sciences Letters*, Vol. 150, pp. 427-441.
- Ring, U., Laws, S., and Bernet, M. (1999). Structural analysis of a complex nappe sequence and late-orogenic basins from the Aegean Island of Samos, Greece. *Journal of Structural Geology*, Vol. 21(11), pp. 1575-1601.
- Ríos, C. and Takasu, A. (2000). P-T conditions of the metamorphic rocks of the Silgará Formation, Santander Massif, Colombian Andes. Abstract, 31st International Geological Congress, August 6-17, 2000, Río de Janeiro, Brazil.
- Ríos, C. (2001). Occurrence, chemical composition and genetic significance of the biotite in the Silgará Formation metamorphic rocks, southwestern Santander Massif, Eastern Cordillera, Colombian Andes. *Boletín de Geología UIS*, Vol. 23(38), pp. 41-49.
- Ríos, C. and García, C. (2001a). First occurrence of the three Al<sub>2</sub>SiO<sub>5</sub> polymorphs in the Silgará

- Formation metapelitic rocks, southwestern Santander Massif, Eastern Cordillera, Colombian Andes. *Boletín de Geología UIS*, Vol. 23(38), pp. 51-59.
- Ríos, C. and García, C. (2001b). Conditions of pressure and temperature of metamorphism in the Santander Massif, Eastern Cordillera, Colombian Andes. Conference, VIII Colombian Congress of Geology, agosto 8-10 de 2001, Manizales, Colombia.
- Ríos, C., García, C., and Takasu, A. (2003a). Tectono-metamorphic evolution of the Silgará Formation metamorphic rocks in the southwestern Santander Massif, Colombian Andes. *Journal of South American Earth Sciences*, Vol. 16, pp. 133-154.
- Ríos, C., Gélvez, J., and Marquez, R. (2003b). Kinetics of the nucleation and growth garnet in the Silgará Formation metapelitic rocks, southwestern Santander Massif. *Boletín de Geología UIS*, Vol. 25(40), pp. 23-38.
- Ríos, C. (2005). Cation substitutions governing the chemistry of amphibole in the Silgará Formation metabasites at the southwestern Santander Massif. *Boletín de Geología UIS*, Vol. 27(2), pp. 13-30.
- Şahin, M.B. and Erkan, Y. (1994). Petrological Features of the Metamorphics of the Yukarıçulhalı-Bağçatak Segment of the Akdağmadeni Massif. *Mineral Res. Expl. Bull.* Vol. 116, pp. 39-46.
- Schäfer, J., Grösser, J., and Rodríguez, G., (1998). Proterozoic Formación Silgará, Cordillera Oriental, Colombia: metamorphism and geochemistry of amphibolites. *Zbl. Geol. Paläont. Teil I*, 1997 (3-6), Stuttgart, pp. 531-546.
- Spear, F. S. (1993). *Metamorphic phase equilibria and Pressure-Temperature-Time paths*. Mineralogical Society of America, Washington, D.C., 799 p.
- Spear, F.S. and Kohn, M.J. (2001). Program GTB: GeoThermoBarometry. Rensselaer Polytechnic Institute. 30 March 2006. [http://ees2.geo.rpi.edu/MetaPetaRen/GTB\\_Prog/GTB.html](http://ees2.geo.rpi.edu/MetaPetaRen/GTB_Prog/GTB.html)
- von Blanckenburg, F. and Davis, J.H. (1995). Slab break-off: a model for syncollisional magmatism and tectonics in the Alps, *Tectonics*, Vol. 14, pp. 120-131.
- Ward, D., Goldsmith, R., Cruz, B., Jaramillo, C., Vargas, L., 1970. Mapa Geológico del Cuadrángulo H-13, Pamplona, Colombia. Ingeominas.
- Ward, D., Goldsmith, R., Cruz, B., Jaramillo, C., y Restrepo, H. (1973). *Geología de los Cuadrángulos H-12, Bucaramanga y H-13, Pamplona, Departamento de Santander*. U.S. Geological Survey e Ingeominas. *Boletín Geológico*, Vol. XXI(1-3), pp. 1-132.
- Weber, M.B.I., Tarney, J., Kempton, P.D. and Kent, R.W. (2002). Crustal make-up of northern Andes: evidence based on deep crustal xenolith suite, Mercaderes, SW Colombia, *Tectonophysics* 345 (1-4), pp. 49-82.
- Yardley, B., 1989. *An Introduction to Metamorphic Petrology*, Longman, Harlow, England, 248 pp.
- Zhao, G. and Cawood, P.A. (1999). Tectonothermal evolution of the Mayuan assemblage in the Cathaysia Block: Implications for Neoproterozoic collision-related assembly of the South China Craton. *American Journal of Science*, Vol. 299, pp. 309-339.